Extraocular muscle stem cells exhibit distinct cellular properties associated with non-muscle molecular signatures

Daniela Di Girolamo, Maria Benavente-Diaz, Melania Murolo, Alexandre Grimaldi, Priscilla Thomas Lopes, Brendan Evano, Mao Kuriki, Stamatia Gioftsidi, Vincent Laville, Jean-Yves Tinevez, et al.

Extraocular muscle stem cells exhibit distinct cellular properties associated with non-muscle molecular signatures

Daniela Di Girolamo[1,2#], Maria Benavente-Diaz[1,2,3#], Melania Murolo[1,2‡], Alexandre Grimaldi[1,2,3‡], Priscilla Thomas Lopes[1,2], Brendan Evano[1,2], Mao Kiruki[1,2], Stamatia Gioftsidi[4,5,6], Vincent Laville[1,2], Jean-Yves Tinevez[7], Gaëlle Letort[8], Sebastian Mella[9], Shahragim Tajbakhsh[1,2*], Glenda Comai[1,2*]

[1]Stem Cells & Development Unit, 25 rue du Dr. Roux, Institut Pasteur, 75015 Paris, France
[2]UMR CNRS 3738, Institut Pasteur, Paris, France
[3]Sorbonne Universités, Complexité du Vivant, F-75005, Paris, France
[4]Université Paris-Est, 77420, Champs-sur- Marne, France
[5]Freie Universität Berlin, 14195, Berlin, Germany
[6]Inserm, IMRB U955-E10, 94000, Créteil, France
[7] Institut Pasteur, Université Paris Cité, Image Analysis Hub, Paris, France
[8] Department of Developmental and Stem Cell Biology, Institut Pasteur, Université de Paris Cité, CNRS UMR 3738, 25 rue du Dr. Roux, 75015 Paris, France
[9] Hub de Bioinformatique et Biostatistique, Cytométrie et Biomarqueurs, Institut Pasteur, 75015 Paris, France

#First co-authors
‡Second co-authors

*Co-corresponding authors

Keywords: muscle stem cell diversity, extraocular muscles, mesenchymal stromal cells, MuSC expansion, MuSC sc-RNAseq, matrisome, TF network

Abstract

Skeletal muscle stem cells (MuSC) are recognized as functionally heterogeneous. Cranial MuSCs are reported to have greater proliferative and regenerative capacity when compared to the ones in the limb. A comprehensive understanding of the mechanisms underlying this functional heterogeneity is lacking. Here we used clonal analysis, live imaging and scRNA-seq to identify critical features that distinguish extraocular (EOM) from limb muscle stem cell populations. A *Myogenin*^{tdTom} reporter showed that the increased proliferation capacity of EOM MuSCs correlates with deferred differentiation and lower expression of the myogenic commitment gene *Myod*. Unexpectedly, *in vitro* activated EOM MuSCs expressed a large array of extracellular matrix components typical of mesenchymal non-muscle cells. Computational analysis underscored a distinct co-regulatory module, which is absent in limb MuSCs, as driver of these features. The EOM transcription factor network, with *Foxc1* as key player, appears to be hardwired to EOM identity as it persists during growth, disease, and *in vitro* after several passages. Our findings shed light on how high-performing MuSCs regulate myogenic commitment by remodeling of their local environment and adopting properties not generally associated with myogenic cells.

INTRODUCTION

Genetic and transcriptomic studies have shown that the MuSC population in any particular anatomical location is heterogeneous. Certain subsets are more prone to self-renewal or differentiation, differ in transplantation efficiency, as well as their stem cell-niche interactions, metabolism, and resistance to stress upon activation (Barruet et al., 2020; Chakkalakal et al., 2014; Dell'Orso et al., 2019; Dumont et al., 2015; Gayraud-Morel et al., 2012; Hernando-Herraez et al., 2019; Micheli et al., 2020; Morree et al., 2019; Ono et al., 2012; Rocheteau et al., 2012; Scaramozza et al., 2019; Tierney et al., 2018; Vartanian et al., 2019; Yartseva et al., 2020; Yennek et al., 2014). Despite this diversity, MuSCs share common functions that are essential for growth and repair (Lepper, 2011; Murphy, 2011; Sambasivan, 2011). Myogenic commitment and differentiation involving *Myod* and *Myog*, respectively, occur in response to injury or growth factors in culture media following isolation of the *Pax7*-expressing MuSCs (Evano and Tajbakhsh, 2018; Zammit et al., 2004).

Unexpectedly, MuSCs in different anatomical locations were found to be programmed with distinct upstream transcription factors (TF) prior to acquiring myogenic identity (Gopalakrishnan et al., 2015; Harel et al., 2009; Kelly et al., 2004; Sambasivan et al., 2009; Tajbakhsh et al., 1997). Extraocular muscles (EOMs) are derived from unsegmented cranial mesoderm and are regulated by distinct transcription factors and signalling molecules compared to the somite-derived limb and trunk muscles (Grimaldi and Tajbakhsh, 2021; Michailovici et al., 2015; Sambasivan et al., 2011). For example, mice lacking the transcription factor *Pitx2* do not form EOMs whereas other cranial and somite derived muscles are unaffected (Diehl et al., 2006; Gage et al., 1999; Zacharias et al., 2011). As some muscle subsets, like the EOMs, are preferentially spared in muscular dystrophies and during ageing (Emery, 2002; Formicola et al., 2014; Verma et al., 2017) and their MuSCs are functionally more robust in terms of proliferation and engraftment efficiency (Stuelsatz et al., 2015), intrinsic properties of MuSCs or myofibers might determine their differentially sensitivity to disease (Randolph and Pavlath, 2015; Terry et al., 2018). Notably, single-cell transcriptomic analysis identified the thyroid hormone signalling pathway as a key factor preventing senescence entry of EOM MuSCs in dystrophin deficient (DMD) rats (Taglietti et al., 2023). Moreover, profiling of EOM MuSCs after heterotopic transplantation into limb muscle showed that, despite significant transcriptional changes, approximately 10% of EOM-specific genes persisted in the ectopic niche (Evano et al., 2020). This finding suggests that cell autonomous regulation of MuSC properties predominates to a certain extent in EOM. Yet, the existence of deeply-rooted TF gene regulatory networks within MuSC subsets and their role in maintaining anatomically distinct phenotypes remains largely unexplored.

Using droplet-based scRNA-seq, we investigated the transcriptional states that govern the outperformance of MuSC subsets. We identified key regulators that confer distinct mesenchymal-like features to activated EOM MuSCs, and extensive expression of extracellular matrix (ECM) components. Activated EOM MuSCs are less prone to differentiation and thus appear to be in a more stem-like state that is maintained *in vitro,* upon passages and *in vivo* during growth, through a specific set of co-regulated transcription factors.

RESULTS

Temporal heterogeneity in myogenic commitment to differentiation among MuSCs

We isolated EOM and *Tibialis anterior* (TA) MuSCs by FACS using *Tg:Pax7-nGFP* mice (Sambasivan et al., 2009) and plated them at the same density to follow up their proliferation and differentiation dynamics (**Figure 1A-B**). Quantification of the number of total and proliferative nuclei (5-Ethynyl-2'-deoxyuridine, EdU uptake, 2h pulse) at D3, D4 and D5 showed a 2.9 to 4.4-fold change increase in EOM compared to TA (**Figure 1C**). However, the percentage of total proliferative cells remained unchanged in both conditions at every time point (**Figure 1D**), arguing that the division probability is equal for EOM and TA. Yet, EOM cultures had twice the percentage of PAX7+ cells and less fusogenic myoblasts compared to TA at later timepoints (D10, **Figure 1E, F**).

We then performed clonal analysis of freshly isolated EOM MuSCs (**Suppl Figure 1A**) and showed that they displayed a 7-fold higher clonal capacity (mean 1315 cells/clone) compared to those from TA (186 cells/clone) (**Suppl Figure 1B,** T1), in agreement with a previous study (Stuelsatz et al., 2015). Surprisingly, the higher clonogenic properties of EOM persisted even when they were pre-amplified for 2 days *in vitro* where they yielded 3656 cells/clone compared to 297 cells/clone for TA (12-fold difference; **Suppl Figure 1B**, T2). Given that EOM and TA MuSCs exhibited a similar proliferative rate in bulk cultures, the clonal data suggests that the greater cellular output of EOM MuSCs is probably due to delayed differentiation. Since *Myog* expression is followed by cell-cycle withdrawal (Andrés and Walsh, 1996; Benavente-Diaz et al., 2021; Guo et al., 1995), a delay in its expression could allow for sustained expansion of EOM MuSCs.

To test this hypothesis, we assessed the differentiation dynamics of EOM and TA MuSCs *in vitro* by live imaging using the *Tg:Pax7-nGFP;Myog*^{ntdTom} mouse line (Benavente-Diaz et al., 2021; Sambasivan et al., 2009), which allowed simultaneous isolation of MuSCs and monitoring of the onset of *Myog* expression by a nuclear tdTOMATO (tdTOM) reporter. Myogenic cells were tracked continuously from D3 and tdTOM intensity scored (**Figure 1G**). TA myogenic cells initiated reporter gene expression earlier than EOM cells (**Figure 1H**). The percentage of tdTOM^{+} cells sharply increased in the TA from 5% at 80h (D3+8hours) post-plating to 40% at 96h (D4). Significantly, only ~7% of EOM cells were tdTOM^{+} by 96h *in vitro* (**Figure 1I**). Western Blot (**Suppl Figure 1C, D**) data were in agreement with the live imaging analysis. For instance, expression of the cell cycle inhibitor *p21*, which regulates cell cycle exit (Guo et al., 1995; Zhang et al., 1999), and expression of phosphorylated p38, which promotes MEF2 transcriptional activity to initiate differentiation (Rugowska et al., 2021), were significantly downregulated in activated EOM MuSCs compared to TA. RT-qPCR showed higher levels of *Myogenin* and *p21* transcripts in TA compared to EOM MuSCs already at D2 (**Figure 1J**). As such, this data suggests that EOM progenitors are less prone to myogenic commitment.

Finally, to test if EOM cells have a global impairment in myogenic differentiation, we used the *Tg:Pax7-nGFP;Myog*^{ntdTom} mice to isolate the stem (PAX7+/GFP+) and committed (MYOG+/tdTOM+) fractions

after D5 *in vitro* (**Figure 1K, Suppl Figure 1E**). No differences were seen by RT-qPCR among EOM and TA tdTOM+ cells for *Myod, Myogenin,* the fusogenic markers *Myomixer* and *Myomaker* (Sampath et al., 2018) and embryonic myosin heavy chain (*Myh3*) indicating that differentiation of EOM cells was not generally impeded (**Figure 1L**). However, plating EOM and TA tdTOM+ myoblasts at high density in differentiation media revealed a lower fusion index and higher percentage of EOM myoblasts incorporating EdU on their last division (**Suppl Figure 1F-H**, (Benavente-Diaz et al., 2021)). Therefore, a general delay in the differentiation of EOM MuSCs appears to contribute to the higher number of myogenic cells (**Suppl Figure 1I**).

Distinct signature of EOM MuSCs upon activation

To understand the phenotypic differences between EOM and TA MuSCs, we performed scRNA-seq of *in vitro* activated MuSCs using the 10x Chromium (**Figure 2A**). Unsupervised clustering divided cells into 2 clusters per sample (**Figure 2B**) that were annotated as progenitors (Prog) or differentiating (Diff) based on myogenic maker expression (**Figure 2B, C**). Notably, EOM progenitors exhibited reduced expression of *Myod* RNA and protein across the entire population at D3 and D5 *in vitro*, thereby suggesting a lower propensity to differentiate (**Figure 2B, Suppl Figure 2A**).

Analysis of differentially expressed genes (DEGs) showed that each cell state had a distinct transcriptional pattern (**Figure 2D, Suppl Table 1**). As expected, TA progenitors expressed a defined Hox-signature (Evano et al., 2020) and inhibitors of differentiation (Id1, Id2, (Jen et al., 1992; Kumar et al., 2009)). EOM and TA differentiating cells shared part of their signature (*Myog, Mymx, Myl4*). However, EOM progenitors displayed markers not been previously noted in MuSCs, such as *Mgp*, *Bgn*, *Col1A2* and *Acta2* (smooth muscle actin) (**Figure 2D**).

We then performed reactome analysis of DEGs (**Figure 2E, Suppl Figure 2B, Suppl Table 2**). As suggested by the DEG heatmap, TA progenitors shared common pathways with the differentiating clusters. Multiple pathways involved in ECM organisation characterised EOM progenitors including “ECM proteoglycans”, “crosslinking of collagen fibrils” and “integrin cell surface interactions”. EOM progenitors were also specifically enriched in Pdgfrβ, a receptor for platelet-derived growth factor, and proteins related to insulin like growth factor binding and integrin signaling (**Figure 2F, Suppl Figure 2C, Suppl Table 3**). Thus, these analyses uncovered a non-canonical signature in EOM progenitors upon activation.

Closer molecular overlap of EOM MuSCs across cell states

We then compared the signature of EOM and TA myogenic progenitors *in vitro* with the quiescent counterparts *in vivo* by scRNA-seq immediately after isolation by FACS (**Figure 3A, B**). While both populations displayed consistent expression of MuSC markers, *Myod* expression was restricted to TA MuSCs (**Figure 3C, D**), suggesting an earlier activation in response to the isolation procedure (Brink et al., 2017; Machado et al., 2017; Velthoven et al., 2017). Differentiation markers like *Myog* were absent

in both populations (**Figure 3C, D**). Visualization of the top 25 most variably expressed genes highlighted distinct transcriptional programs of EOM and TA quiescent clusters (**Figure 3E, Suppl Table 4**). Moreover, microarray analysis showed that EOM quiescent MuSCs also stand appart from those in other cranial-mesoderm derived muscles, such as the esophagus and masseter (**Suppl Figure 3A**).

Interestingly, we found several conserved genes between the quiescent and activated sc-RNAseq states at each anatomical location, while others were unique to the quiescent or activated cell states (**Figure 3F-I**). EOM genes unique to the quiescent state included *Tshr*, encoding the thyroid-stimulating hormone receptor, previously recognized in bulk RNAseq as "EOM-resistant", i.e. retained following engraftment into the limb (Evano et al., 2020), and shown to prevent senescence in EOM MuSCs of DMD rats (Taglietti et al., 2023). Matrix Gla protein (Mgp), a critical regulator of angiogenesis in multiple organs (Kida and Yamaguchi, 2022), was exclusively upregulated in EOM cells upon activation (**Figure 3H**). Amongst the conserved EOM genes across cell states we identified *Pitx2*, a major upstream regulator of EOM development (Gage et al., 1999), *Fos*, which labels a subset of limb MuSCs with enhanced regenerative capacity (Almada et al., 2021) and *Foxc1,* which is involved in ocular development (Smith et al., 2000) and reported to regulate the balance between myogenic and vascular lineages within somites (Lagha et al., 2009; Mayeuf-Louchart et al., 2016) (**Suppl Figure 3B**). The EOM signature also featured *Igfbp7*, a specific marker of quiescent MuSCs (Fukada et al., 2007) that is upregulated upon exercise (Chen et al., 2020) (**Figure 3F, Suppl Figure 3B, C**). Additionally, the EOM common signature encompassed several ECM components and regulators (e.g. *Bgn*, *Loxl1*, *Col1a2*, *Col6a1*), TFs associated with fibrosis and connective tissue development (e.g. *Foxp1* (Grimaldi et al., 2022; Shao and Wei, 2018), *Egr1* (Havis and Duprez, 2020)) and *Acta2* (alpha smooth muscle actin), a marker of smooth muscle, fibroadipogenic progenitors (Joe et al., 2010; Uezumi et al., 2010) and smooth muscle-mesenchymal cells (SMMCs, (Giordani et al., 2019)) (**Figure 3F, H**).

In the TA, *Lbx1, Vgll2* and *Hox* genes were found as common signature throughout cell states (**Figure 3G,I; Suppl Figure 3B, C**). *Lbx1* is a homeobox transcription factor required for the migration of myogenic progenitor cells to the limbs (Brohmann et al., 2000; Gross et al., 2000) and *Vgll2* (previously Vito-1) is a key cofactor of the myogenic differentiation program (Günther et al., 2004; Maeda et al., 2002). *Lbx1, Vgll2* and *several Hox* genes had been already identified in the limb both at the MuSC level and in entire muscles in the adult (Evano et al., 2020; Honda et al., 2017; Terry et al., 2018) (**Figure 3I**).

Altogether, our analysis revealed a closer molecular overlap for EOM MuSCs across cell states (quiescence vs *in vitro* activation), including several TFs and ECM markers that were distinct from TA MuSCs.

Activation of EOM MuSCs involves extensive ECM remodelling

Given the well-established role of ECM synthesis and remodelling on MuSC proliferation and self-renewal (Baghdadi et al., 2018; Rayagiri et al., 2018; Tierney et al., 2016; Yin et al., 2013), we examined these features using Matrisome database (Matrisome DB), which compiles *in silico* and experimental

data on ECM constituents (Naba et al., 2015). We identified components of the Matrisome DB present in our single-cell dataset and created a global score for ECM component expression (**Figure 4A**) (see Methods). Significantly, the EOM progenitor cluster had the highest matrisome score (**Figure 4A**) and expressed the highest number of genes for each matrisome category (**Figure 4B**).

We then validated some matrisome candidate genes by immunofluorescence or Western blot on *in vitro* activated EOM and TA MuSCs (**Figure 4C-D**). EOM progenitors expressed higher levels of Fibronectin (FN1), which promotes MuSC expansion in a cell autonomous manner (Bentzinger et al., 2013), Collagen I (COLI), a major component of the fibrotic ECM (Dulauroy et al., 2012) shown to suppress differentiation of C2C12 cells (Alexakis et al., 2007) and Collagen IV (COLIV), which is secreted by MuSCs as well as myoblasts and fibroblasts in culture (Baghdadi et al., 2018; Kühl et al., 1984) (**Figure 4C**). In addition, EOM progenitors also displayed differential expression of PDGFRβ, a gene identified on the EOM molecular functions (**Suppl Figure 2C**). PDGFRβ is a tyrosine-kinase receptor commonly expressed by mesenchymal cells and pericytes (Hellström et al., 1999; Levéen et al., 1994; Soriano, 1994) (**Figure 4C**). Interestingly, Pdgfrβ and Acta2 are markers of Smooth Muscle-Mesenchymal Cells (SMMCs), a novel Itga7+ Vcam- Pdgfrb+ Acta2+ cell subpopulation present in adult muscle that exhibits myogenic potential and promotes MuSC engraftment following transplantation (Giordani et al., 2019).

Western blot analysis confirmed that EOM progenitors produce higher levels of Caveolin1 (CAV1) and CAVIN1 (**Figure 4D**), which are co-expressed in caveolae and downregulated upon differentiation of rhabdomyosarcoma cells (Faggi et al., 2015). CAV1 is a marker of quiescent and Pax7+ activated mouse MuSCs (Gnocchi et al., 2009) whereas in human, CAV1+ MuSCs are associated with ECM organization, expression of quiescent markers, and increased engraftment capacity (Barruet et al., 2020). SPARC, MGP and IGFBP7 were also upregulated in EOM activated MuSCs (**Figure 4D**). Their activity appears to be context dependent as they promote or suppress proliferation in different cell types (Ahmad et al., 2017; Artico et al., 2021; Cho et al., 2000; Jing et al., 2019; Li et al., 2020; Melouane et al., 2018). Given the large number of matrisome genes characterising EOM progenitors, we examined the expression of MMP2, a matrix remodelling protein (Gonçalves et al., 2022) whose activation increases the proportion and mobility of Pax7+ cells (Mu et al., 2010). As expected, an enrichment of the active form of MMP2 was observed in EOM progenitors. TA progenitors displayed instead an enrichment of the pro-MMP2 or latent form (**Figure 4D)**.

In parallel, we assessed to what extent activated EOM MuSCs resemble other cells in skeletal muscle displaying mesenchymal features (**Suppl Figure 4A, Suppl Table 5**). Notably, EOM progenitors displayed a higher score for SMMCs (Giordani et al., 2019), FAPs (Oprescu et al., 2020), myotendinous junction B myonuclei (Kim et al., 2020), Twist2+ cells (Liu et al., 2017), fetal MuSCs (Tierney et al., 2016), developing limb connective tissues (Lima et al., 2021) and the skeletal muscle mesenchyme subpopulation identified in human fetal limb (Xi et al., 2020). In contrast, TA progenitors displayed a higher score for myogenic commitment and differentiation (**Suppl Figure 4A**).

Finally, we focused on PDGFRβ, for which FACS antibodies exist, to validate the potential link between mesenchymal EOM features and *in vitro* expansion capacity. Flow cytometry analysis corroborated the scRNA-seq and immunofluorescence data, where PDGFRβ was enriched in EOM samples (**Suppl Figure 4B, C**). To distinguish the functional properties of PDGFRβ+ and PDGFRβ- cells, we pulsed them with EdU (**Figure 4G**). Notably, PDGFRβ+ cells had a significantly higher proliferative capacity (**Figure 4H-J**). While the percentage of MYOD+ cells was unchanged between the two cell populations, MYOG was much more abundant in the PDGFRβ- fraction (**Figure 4K, L**). Therefore, the PDGFRβ+ myoblasts are characterised by a higher proliferative potential and decreased differentiation status. Altogether, our analysis showed that EOM progenitors have an unusual transcriptome profile, express a wide range of ECM-related factors, and harbour a mesenchymal signature.

EOM transcriptome profile is associated with a unique transcription factor network

To further investigate myoblast heterogeneity, we inferred single cell regulatory networks using pySCENIC (Aibar et al., 2017; Sande et al., 2020) where co-expression patterns and transcription factor binding motifs identify 'regulons" (transcription factors and putative targets) (**Figure 5A, Suppl Table 6**). As expected, regulons associated with myoblast differentiation such as *Myod*, *Myog* and *Mef2* family were specifically active in differentiated cells of EOM and TA (**Figure 5B**). Of note, the top 5 regulons of TA progenitors were also found to be active in EOM progenitors, whereas the top 5 regulons of EOM progenitors were unique to this cluster (**Figure 5B**). EOM progenitors displayed unique regulons involved in connective tissue and ECM remodelling including *Egr1* (Havis and Duprez, 2020) and *Creb3l1*, a downstream effector of thyroid hormone signaling (García et al., 2017; Sampieri et al., 2019). Top regulons of EOM progenitors are also involved in cell proliferation (*Foxc1* (Yang et al., 2017), *Sox4* (Moreno, 2019), *Fos* (Almada et al., 2021), *Klf6* (Dionyssiou et al., 2013), *Ebf1* (György et al., 2012)), commitment into endothelial and smooth muscle fates (*Foxc1* (Han et al., 2017; Mayeuf-Louchart et al., 2016; Whitesell et al., 2019; Yang et al., 2017)) as well as differentiation into mesenchymal lineages (Ebf1, (El-Magd et al., 2021; Jimenez et al., 2007; Pagani et al., 2021). Of note, some EOM regulons were already enriched in quiescent EOM MuSCs, and their expression was upregulated upon activation (**Suppl Figure 5A, B**).

We then built a network restricted to transcription factors (**Figure 5C)**, where each node (circle) is an active transcription factor and each edge (distance between nodes) is an inferred regulation between 2 transcription factors (Grimaldi et al., 2022). When placed in a force-directed environment (see Methods), these nodes aggregated based on the number of shared edges thereby highlighting associated and co-regulating transcription factor modules. Strikingly, the transcription factors of the most specific regulons of each cluster preferentially organised as tightly related modules (**Figure 5C**). In agreement with our previous analyses, known co-regulating transcription factors in differentiated cells (*Myod, Myog, Mef2a, Mef2c, Myf6*) formed a tight module (**Figure 5C)**. The TA module was composed of genes required for limb embryonic development (*Hox* genes, *Lbx1*) (Gross et al., 2000; Swinehart et al., 2013), where *Hoxa11*, is a determinant of embryonic limb identity (Zakany and Duboule, 2007), and HoxA and HoxC

clusters are signatures of adult TA MuSCs (Evano et al., 2020; Yoshioka et al., 2021) (**Figure 5C**, **Suppl Figure 5B**).

The EOM module included *Foxc1, Egr1*, *Creb3l1*, *Dmrta2*, *Sox4*, *Fos* and *Egr1* together with *Pax7* and *Hes1* which support MuSC quiescence (Baghdadi et al., 2018; Mourikis et al., 2012; Olguin and Olwin, 2004; Relaix and Zammit, 2012). However, this network persists in proliferating EOM progenitors as assessed by the higher levels of PAX7, CCND1 (Cyclin D1), together with EOM TFs (FOXC1, EBF1 and CREB3L1) at the protein level (**Suppl Figure 5C, D**). Although *Fos* and *Egr1* act as stress signatures following tissue dissociation (Machado et al., 2021) in our dataset, the expression of these genes (i.e. the StressIndex) correlated with *Pax7* expression and anti-correlated with *Myod* (**Suppl Figure 5E, F**). Regression of the StressIndex or removal of these genes did not alter the general aspect of the data (**Suppl Figure 5G)**, pointing at a role for these genes also in the EOM progenitor maintenance.

EOM features are present during the growth phase *in vivo* and retained upon passages *in vitro*

Given that EOM MuSCs possess an unusual transcriptomic state and delayed myogenic commitment, we examined these features following passage of MuSCs isolated from *Tg:Pax7-nGFP;Myog*^{ntdTom} *in vitro* (**Figure 6A, Suppl Figure 6A, B**). While the total cell number was reduced with passages for both EOM and TA (**Suppl Fig 6A, B**), the normalised cellular output was consistently higher for the EOM and correlated with a lower tdTOM/GFP ratio (**Figure 6B, C**). Real-time qPCR and protein analysis showed that expression of *Pax7* and *Hey1*, a bHLH transcription factor that is required for MuSC maintenance (Noguchi et al., 2019), EOM specific regulon TFs (*Foxc1*, *Sox4*, *Ebf1*, Creb3l1) and genes identified by the matrisome or molecular functions (*Bgn*, *Sparc*, *Igfbp2*, *Igfbp7*, *Pdgfrb*) were all retained or even increased in whole EOM cell populations (mix of GFP+ and tdTOM+ cells) after several passages (Figure 6D-G), and specifically in the GFP+ fraction (**Suppl Figure 6C-E**). These results show that EOM MuSCs cells retain a cell autonomous non-canonical signature that is hard-wired even after extended cell culture and that is not present in the TA.

Next, we assessed whether EOM progenitor features were already present in their activated state *in vivo*, for instance, in fetal development and postnatal stages, where extensive muscle growth and myogenic cell expansion occurs (Gattazzo et al., 2020a; Relaix and Zammit, 2012) or if these features were only acquired in adulthood upon reactivation from the quiescent state *in vitro*. First, we isolated EOM and TA MuSCs at E18.5 and P21 and showed that here too, EOM cells were less differentiated upon activation *in vitro* (**Suppl Figure 7A**). Then, we examined activated MuSCs directly *in vivo* by RT-qPCR. Given that GFP protein persists during myogenic commitment (Sambasivan et al., 2009) and this might introduce a bias in the initial populations, we isolated by GFP+/tdTOM- fractions from *Tg:Pax7-nGFP;Myog*^{ntdTom} mice at P7-P10 (**Figure 7A, Suppl Figure 7B**). Similarly, to the *in vitro* sc-RNAseq data, RT-qPCR revealed significantly lower levels of *Myogenin* and higher transcript levels for EOM specific regulon TFs (*Foxc1*, *Ebf1*, *Sox4*, *Creb3l1*) and matrisome components on the activated EOM progenitors (**Figure 7B**). Together with our live-imaging (Figure 1G-I), FACS (Suppl Figure 1E) and sc-

RNAseq data (Figure 2), this analysis suggests that EOM MuSCs repress myogenic commitment and appear to maintain a more "stem-like" state upon activation, and this property is conserved from development to adulthood.

Foxc1 marks the EOM MuSC lineage and plays a role in progenitor cell maintenance

We then focused on *Foxc1* for further analysis as it is one of the top regulons and DEG of the activated and quiescent sc-RNAseq dataset (**Figure 5 A, B, Suppl Figure 3B, Suppl Figure 5B, D**) and we previously identified *Foxc1* as a DEG and top regulon of EOM progenitors in the early embryo (E11.5,(Grimaldi et al., 2022)). Notably, bulk RNAseq (Terry et al., 2018) also showed higher *Foxc1* expression in entire EOMs compared to other adult muscle groups (**Suppl Fig 7C**). As such, *Foxc1* is a good candidate for determining EOM properties throughout the myogenic lineage continuum and across developmental states.

First, we validated FOXC1 protein expression *in vivo* and *in vitro.* As expected, immunostaining on tissue sections of E12.5 $Myf5^{Cre};R26^{tdTom}$ embryos showed expression of FOXC1 in 54.7% of EOM myogenic progenitors but not in limb, back, nor masseter muscles (**Suppl Figure 7D, E**). Analysis of $Pax7^{CreERT2};R26^{tdTom}$ mice showed FOXC1 expression in postnatal (P10) and adult EOM MuSCs (**Figure 7C-E**) but not in the TA muscles. FOXC1 was strongly expressed in adult EOM MuSC cultures (**Suppl Figure 7F-H**). FOXC1 was expressed in about 75% of PAX7+ cells at D5, expression was progressively lost during differentiation and the majority of the FOXC1+ cells incorporated EdU at every time point (**Suppl Figure 7I, J**). Thus, differences in *Foxc1* expression between the EOM and TA appear to arise during development and persist upon activation.

As differences in *Myogenin* mRNA between EOM and TA were already evident at D2 following *in vitro* activation (**Figure 1J**), we used this early timepoint to functionally validate a potential role for *Foxc1* in progenitor maintenance. Thus, we silenced *Foxc1* using siRNA in EOM MuSCs right after FACS (**Suppl Figure 7K**). The total cell number and percentage of PAX7+ cells were not changed 2 days after silencing, despite effective downregulation of FOXC1 at the protein level (**Suppl Figure 7L-L'''**) and transcript level (**Suppl Figure 7M**). Yet, a 2.7-fold increase in *Myogenin* expression was detected by RT-qPCR following silencing (**Suppl Figure 7M'**). Given that the effect of siRNAs was only transient, we transduced EOM activated MuSCs with lentiviruses expressing different short-hairpin RNAs (shRNA) against *Foxc1* to be able to examine later timepoints (Suppl **Figure 7N**). Immunofluorescence and EdU uptake at D5 showed an efficient depletion of FOXC1 protein, and concomitant severe reduction in the total cell number and percentage of EdU+ cells (Suppl **Figure 7O-P**). While lower number of myotubes were formed in shRNA FOXC1 TA cells, the fusion index was not significantly different (**Suppl Figure 7Q, R**).

To assess if *Foxc1* would confer some EOM features to TA, we overexpressed this gene in activated TA MuSCs cells (**Figure 7F**) using gain-of-function (GOF) FOXC1 lentiviruses carrying mCherry as reporter that allow to re-isolate the transduced cells (**Figure 7G, H**). Notably, there was robust

upregulation of FOXC1 (15-30x) at D5 (**Figure 7I, J, K', N**) and many *Foxc1* direct targets (**Suppl Table 7**), including matrisome components (e.g. *Sparc*, *Pdgfrβ*, *Fbn1*) and other EOM specific regulon TFs (e.g. *Ebf1*, *Creb3l1*, *Egr1)*. Properties of re-isolated GOF cells (**Figure 7K-Q**) included a larger cellular and nuclear area (**Figure 7K, K', O**) and less fusogenic potential (**Figure 7L, M**). Unexpectedly, FOXC1 overexpression also resulted in downregulation of *Pax7* and *Myod*, less cells/well and reduced EdU uptake (**Figure 7J, P, Q**). These phenotypes might be the result of strong overexpression and cells acquiring a strong mesenchymal character. We thus investigated the FOXC1 GOF condition in "mixed cultures" which contain transduced (FOXC1+mCherry+) and non-transduced (FOXC1-mCherry-) TA cells (**Figure 7F, R-Y**). This strategy allowed us to assess the effect of secreted factors produced by FOXC1+ cells on non-transduced cells. As expected for mixed cultures, FOXC1 fluorescence intensity showed a bimodal distribution, with one population being as negative control and the other expressing high levels of the protein (**Figure 7R**). Interestingly, the total number of nuclei in the mixed GOF wells was higher than controls (**Figure 7T**), which contrasts with the result in pure GOF cultures (**Figure 7P**). Thus, we evaluated the individual cellular properties of transduced and non transduced cells in the mixed GOF cultures. While FOXC1+ cells showed higher nuclear area and reduced EdU uptake as in pure GOF cultures, overexpression of FOXC1 led to an augmentation in both the number and percentage of proliferating cells within the non-transduced population (compare FOXC1+/- subpopulations in **Figure 7S, U** with **Figure 7O, Q**).

Finally, we performed live imaging on FOXC1 GOF mixed cultures (**Figure 7F**). While starting with control and GOF cultures with similar transduction efficiencies (88% and 80% mCherry+ cells at 12h, respectively) (**Figure 7V**), we found that the density of mCherry+ cells in GOF wells was reduced by half of that of control wells by 48h (**Figure 7X, Movie 1** and **2**), with a concomitant increase in the density of mCherry- cells (**Figure 7Y, Movie 1** and **2**).

Therefore, our data suggest a role for the FOXC1-induced secretome in cell proliferation of adjacent cells (**Figure 7Z**). Importantly, overexpression of *Creb3l1*, another EOM regulon TF, in TA MuSCs (**Suppl Figure 7S**) did not show alterations in *Pax7, Myod*, most matrisome genes examined, nor the cellular properties (**Suppl Figure 7S-Z**). Altogether, our findings support the notion that physiological levels of *Foxc1* in EOM MuSCs may allow their maintenance in a progenitor like state, likely through secreted factors.

Transcription dynamics expose EOM and TA disparities in progenitor-state maintenance

We then performed more detailed bioinformatic analysis of the matrisome by correlating the number of matrisome-driving regulons between EOM and TA upon activation (**Figure 8A-C, Suppl Table 8**). EOM MuSCs consistently regulated a higher number of matrisome genes than TA cells (**Figure 8A**). The ratio of the number of regulations of matrisome genes between EOM and TA activated MuSCs showed that the difference was maximal when considering the top 5 regulons, including as expected *Foxc1* together with *Alx4*, *Dmrta2*, *Zmiz1* and *Fos* (**Figure 8B, C**). Interestingly, *Foxc1*, *Dmrta2* and *Fos* were also active regulons in quiescence, with slight disparities between EOM and TA (**Suppl Table 9**).

Next, we set out to determine whether matrix genes underlie the transition towards progenitors and committed cells during activation using scVelo (Bergen et al., 2020). This method computes local changes in the relative number of unspliced/spliced variants (Manno et al., 2018) and identifies candidate "driver genes", i.e. most transcriptionally dynamic and responsible for the inferred velocity (**Figure 8D, E**). Two distinct velocity streams stood out in both datasets, towards differentiation (*Myog*^{High}) and towards a progenitor-state (*Pax7*^{High}). Strikingly, a larger fraction of EOM cells appeared to transition towards a progenitor state compared to TA (**Figure 8D, E**). These trajectories did not appear to be specifically correlated with cell cycle phases (**Suppl Figure 8 A, B**), which was shown to influence transcriptomic data in some cases (McDavid et al., 2016). Hence, the velocity streams observed are most likely reflect transitions between distinct cell states instead of the cell cycle progression of a homogeneous cell state.

Using scVelo built-in functions, we extracted the top driver genes underlying the velocity towards the progenitor state in both datasets (**Figure 8F-G, Suppl Table 10, 11**). Out of the top 100 driver genes, 30 were common to both datasets, including *Col5a1*, which plays a critical role in maintenance of quiescence (Baghdadi et al., 2018) (**Figure 8F,G**). Interestingly, several matrisome components including *Fn1*, other collagens, and *Igfbp7* (Insulin growth factor binding protein 7), were unique to EOM. Of note, IGFBPs bind and regulate insulin-like growth factors (IGFs) thereby repressing myogenic differentiation but they also have IGF-independent activity (Clemmons, 1997; Engert et al., 1996; Jin et al., 2020). GO molecular functions associated with these driver genes during myogenic progenitor maintenance showed that this transition was characterised by active upregulation of ECM components specifically in EOM, in agreement with our previous results (**Suppl Figure 8C**).

We then performed conditioned media (CM) exchange experiments to gain functional insights into the role of EOM secreted factors by culturing hindlimb cells in presence of EOM-CM, TA-CM or control media for 3 days (**Figure 8H**). In agreement with the FOXC1 GOF experiments (**Figure 7R-Z**) EOM-CM induced a ~5x increase in the total number of nuclei/well, whereas no significant differences were observed with TA-CM and control media (**Figure 8I**). Further, the percentage of EdU+ cells remained unchanged (**Figure 8J**) suggesting that EOM secreted factors may delay differentiation.

To assess if mesenchymal features of EOM cells were recapitulated *in vivo,* we asked whether bipotent myogenic progenitors that we previously identified in EOM to give rise to myogenic and connective tissue cells during embryogenesis (Grimaldi et al., 2022) persisted postnatally. Examination of *Myf5*^{nlacZ}*:Pdgfra*^{H2BGFP} mice, where *Myf5*^{nlacZ} allows tracing myogenic progenitors and progeny, and GFP labels mesenchymal connective tissue cells, confirmed the presence of βgal+/GFP+ cells in the EOM but not in masseter and tongue muscles in the head (**Figure 8K, L**). Surprisingly, analysis of EOM and TA MuSCs and fibroadipogenic cells (FAPs) identified a hybrid population positive for both Sca-1 (FAPS marker, (Joe et al., 2010)) and GFP, only in EOM samples (8% of total GFP+ population; **Suppl Figure 8D-F**). We then isolated FAPS, MuSCs, and the SCA-1+GFP+ cells from the EOM, and performed RT-qPCR, for *Pdfgra*, *Pdgfrb* and *Col1a2* (**Suppl Figure 8G**). Notably, the Sca-1+GFP+ progenitor population showed an intermediate pattern of expression of these matrisome genes between that of

MuSCs and FAPS, suggesting a mesenchymal signature that exclusively belongs to EOM MuSCs subsets. Finally, differential gene expression analysis of a publicly available sc-RNAseq dataset filtering on our EOM-specific regulon TFs, highlighted *Egr1* and *Foxc1* as upregulated in dystrophic EOM (**Suppl Figure 8H**), a condition where EOM MuSCs were described to be proliferative (Taglietti et al., 2023). Altogether, this *in vivo* data corroborated the results obtained by bioinformatic analysis on our *in vitro* activated MuSC dataset.

DISCUSSION

An unusual feature of skeletal muscle stem cells is their reliance on distinct gene regulatory networks (GRNs) in different anatomical locations. Most studies on myogenesis have focused on trunk and limb muscles and only a handful of transcription factors and signalling pathways have been identified as hallmarks of specific muscle groups. Here, we used multiple approaches and identify unusual features and specific GRNs that functionally distinguish EOM from TA MuSCs.

EOM MuSCs are more refractory to *in vitro* differentiation

By monitoring *Myog* and *Myod* expression, we showed that EOM MuSCs have a lower propensity to differentiate following activation and persist as a proliferative population. Given the pivotal role of *Myod* in commitment and differentiation (Vicente-García et al., 2022), the lower levels of *Myod* transcript and protein in activated EOM MuSCs even upon upregulation of the $Myog^{tdTom}$ reporter is intriguing and deserves further investigation. As foetal and early postnatal EOM MuSCs are also refractory to differentiation, we propose that this property might be hardwired by unique GRNs that are retained throughout development and adulthood. Notably, trunk foetal MuSCs were shown to be more resistant to myogenic progression upon *in vitro* expansion and contribute more efficiently upon transplantion than the adult counterparts (Sakai et al., 2013; Tierney et al., 2016). In addition, limb MuSCs cells isolated at birth displayed prolonged expansion and delayed fusion compared with those in the adult (Gattazzo et al., 2020b). Similarly, EOM MuSCs showed a reduced fusion index compared to those in adult limb. Altogether our data suggest that EOM MuSCs retain features of respective foetal and neonatal myogenic cells.

Major obstacles for cell-based therapies are the large cell numbers required for transplantation and the fact that ex vivo amplification of somite-derived MuSCs leads to a drastic decline in regenerative potential due to commitment to differentiation (Briggs and Morgan, 2013; Ikemoto et al., 2007; Montarras et al., 2005). While significant progress has been made (Charville et al., 2015; Ishii et al., 2018; L'honoré et al., 2018; Xie et al., 2021), the identification of factors that regulate cell fate decisions in distinct MuSC populations is another resource for advancing knowledge in this context.

EOM progenitors exhibit a mesenchymal genetic signature upon activation

scRNA-seq analyses provided some insights into the transcriptional landscape regulating MuSC quiescence, activation and self-renewal in somite-derived muscles (Dell'Orso et al., 2019; Hernando-

Herraez et al., 2019; Machado et al., 2021; Micheli et al., 2020; Yartseva et al., 2020). For cranial MuSCs, our scRNA-seq analysis of activated EOM and TA MuSCs showed distinct transcriptional profiles that divided myoblasts into two subpopulations: those that resembled progenitors and those differentiating. The EOM progenitor population was characterised by higher *Pax7*, reminiscent of *in vitro* reserve cells (Laumonier et al., 2017; Yoshida et al., 1998; Zammit et al., 2004) and ontology analysis of its DEGs showed an enrichment in ECM organisation processes and *Pdgf* signalling.

Transcriptomic analysis of trunk MuSCs highlighted a dynamic profile of Pdgf ligands and receptors during myogenesis (Contreras et al., 2021). Treatment with NOTCH and PDGFRβ ligands (DLL4 and PDGF-BB respectively) enhanced migration, expression of stem cell markers and perivascular-like features in MuSCs (Gerli et al., 2019) and embryonic myoblasts (Cappellari et al., 2013). Notably also, heterogeneity of activated MuSCs was noted during regeneration, including a transitional Notch2-high state and an ECM-high state that regulates self-renewal (Yartseva et al., 2020). As PDGFRβ and several Notch pathway components (e.g. Notch1, Notch3, Hey1) are co-expressed in activated EOM progenitors, and at significantly higher levels than in TA muscle, we speculate that cross-talk between these pathways could take place in this subpopulation.

Putative role of ECM secretion and remodelling by activated EOM MuSCs

Self-renewal in the muscle lineage is dependent on cell-autonomous expression, deposition, and remodelling of ECM components such as Fibronectin (Bentzinger et al., 2013; Lukjanenko et al., 2016; Tierney et al., 2016), Col VI (Urciuolo et al., 2013) and Laminin-α1 (Rayagiri et al., 2018). EOM progenitors relate more to fetal MuSCs with respect to enrichment in matrisome components such as Fn1, Fbn1, Vcam and collagens (Tierney et al., 2016). Notably, an extensive and more complex ECM is obervsed in EOMs *in vivo* (McLoon et al., 2018). Therefore, we hypothesize that *in vitro* activated EOM MuSCs secrete high amounts of ECM and self-autonomously maintain stemness when removed from their niche. For instance, FAPs exert a supportive role in myogenesis by secreted matrix and cytokine components (Joe et al., 2010; Kotsaris et al., 2023; Murphy et al., 2011; Uezumi et al., 2014). Myogenic cells expressing mesenchymal markers were also reported in human embryos and from human iPSCs *in vitro* (Xi et al., 2020). In the EOM, this plasticity was observed *in vivo*, where EOM myogenic progenitors transition towards non-myogenic cell fates (Grimaldi et al., 2022). Here, we have extended these observations to the early postnatal period, where considerable proliferation and fusion occurs. We did so by using using *Pdgfra*^{H2BGFP};*Myf5*^{nlacZ} mice and the identification of a subpopulation of EOM GFP+ cells co-expressing the mesenchymal stem cell marker SCA-1 *in vivo*, which is normally used as a negative marker of MuSCs (Liu et al., 2015).

A unique network of transcription factors maintains EOM progenitors

Most head regulon genes that we identified in EOM progenitors are not typical myogenic TFs. One of the most active regulons was *Foxc1*, a pro-mitogenic factor in cancer (Yang et al., 2017) and driver of endothelial/smooth muscle fates (Lagha et al., 2009; Mayeuf-Louchart et al., 2016; Whitesell et al.,

2019). Another top regulon was *Egr1*, which promotes expression of many ECM-related genes (Gaut et al., 2016; Milet et al., 2017). Interestingly, *Foxc1* and *Ebf1* are active transcription factors underlying the transition of myogenic towards non-myogenic cell fates in embryonic EOM (Grimaldi et al., 2022). As *Foxc1* is expressed in quiescent and activated EOM MuSCs, this gene might reinforce a progenitor/stem-cell identity throughout the lineage. Interestingly, FOXC1 overexpression in TA MuSCs resulted in upregulation of *Egr1* and downregulation of *Ebf1* in support our bioinformatic analysis indicating that these TFs form a co-regulatory module.

As predicted by our analysis *in silico*, FOXC1 overexpression in TA MuSCs upregulated several EOM matrisome components and downregulated *Myod,* in accordance with a previous study (Wright et al., 2021), thereby promoting a less committed state. Given that *Pitx2* appears as a target of *Foxc1* in our studies (Suppl Table 7) and its overexpression promotes MuSC proliferation and enhances the regenerative potential of dystrophic MuSCs (Vallejo et al., 2018), we expected an increase in the nuclear output when overexpressed in TA MuSCs. Yet, we observed the opposite phenotype in pure TA GOF cultures, thereby raising several possibilities. First, it was reported that sustained expression of FOXC1 can induce stem cell quiescence in the skin (Lay et al., 2016; Wang et al., 2016). Alternatively, a strong upregulation of FOXC1 might have induced an irreversible drift towards a mesenchymal phenotype in hindlimb MuSCs as denoted by the reduced expression of *Pax7*. Yet, our mixed GOF cultures also suggest that the FOXC1-dependent secretome can promote proliferation of adjacent non-transduced cells. Finally, as *Foxc1* is part of a co-regulatory module in the EOM its singular overexpression might not be sufficient to confer the full EOM phenotype to limb cells. Future studies should assess the role of this TF in EOM progenitor emergence and disease.

Conclusion

Using in-depth bioinformatic analysis, *in vitro* approaches, and analysis of expression patterns *in vivo*, we propose a model where the outperformance of EOM MuSCs depends on the expression of a tightly associated module of transcription factors regulating a distinct pattern of ECM-remodelling factors, cell receptors and growth factor binding proteins. These components define the pace at which EOM MuSCs progress through the myogenic lineage and maintenance of a stem-like population. As such, our study lays the groundwork for elucidating the mechanisms of selective sparing of muscle groups in dystrophic disease by providing information on a unique core GRN within this muscle group.

Materials and methods

Animal care

Animals were handled according to national and European Community guidelines and an ethics committee of the Institut Pasteur (CETEA) in France approved protocols. Except when indicated otherwise, males and females of 2-4 months were used. *Tg:Pax7-nGFP* (Sambasivan et al., 2009), *Myf5*^{Cre} (Haldar et al., 2007), *Myf5*^{nlacZ} (Tajbakhsh et al., 1996) *Myog*^{ntdTom} (Benavente-Diaz et al., 2021),

Pdgfra^{H2BGFP} (Hamilton et al., 2003), *Pax7*^{CreERT2} (Mathew et al., 2011) and *R26*^{tdTom} (Madisen et al., 2009) mouse lines were maintained in a C57Bl/6JRj background. To induce recombination of *Pax7*^{CreERT2}*:R26*^{tdTom} mice a 20 mg/ml stock solution of Tamoxifen was prepared in 5% ethanol and 95% sunflower seed oil by thorough resuspension with rocking at 4 °C. For adult mice, 2 mg of tamoxifen (Sigma #T5648) were administered by gavage during 5 consecutive days and animals sacrificed 5 days later. To induce recombination of pups, the Tamoxifen stock solution was diluted to 15mg/ml with sunflower seed oil and 0.15 mg were administered daily by subcutaneous injection between P4 and P6 daily. Pups were sacrificed at P10 by decapitation and adult mice by cervical dislocation.

Muscle stem cell culture, treatment and transfection

MuSC isolation was performed as described (Gayraud-Morel et al., 2017) with some modifications indicated in Supplemental Methods. Cells isolated by FACS were cytospun (3 min at 50g at RT) and plated onto Matrigel® (Corning, 354248) coated dishes and cultured in growth media at 3% O2, 5% CO2, 37°C for the indicated time. Half volume of media was changed every second or third day. To assess proliferation, cells were pulsed with 10^{-6} M of EdU (ThermoFisher, C10640) in cell culture media for 2h prior to fixation. To induce myogenic differentiation and fusion, myoblasts were plated at high density (33,000 in Figure 7M, Suppl Figure 7R, Z or 75,000 cells/cm^2 in Suppl Figure 1H) onto Matrigel-coated plates in the growth medium. Once adherent, cells were changed to differentiation medium (DMEM with 5% serum and 1% P/S).

Conditioned media (CM) experiment were performed isolating EOM and TA MuSCs by FACS based on GFP fluorescence from *Tg:Pax7-nGFP* mice, and collecting the media 3 days post plating. Hindlimb MuSCs were cultured in growth media (control) or treated with CM from day 1 to day 4 post plating before analysis.

For loss of function experiments, freshly isolated satellite cells from *Tg:Pax7-nGFP* mice were transfected in suspension immediately after FACS with the ON-TARGET plus SMARTpool against FOXC1 (Dharmacon, L-047399-01-0005) or Scramble (Dharmacon, ON-TARGETplus Non-targeting Control siRNA, D0018100205) at 200 nM final concentration using Lipofectamine 3000 (ThermoFisher, L3000001) in Opti-MEM (Fisher Scientific, 11564506) as described by the manufacturer. Briefly, a pre-mix of siRNA/Optimem (1.5ul /20ul) and Lipofectamine3000/Optimem (0.3ul / 20ul) were incubated separately 5 min RT, mixed at 1:1 ratio and incubated 15 min more at RT. 2.10^4 cells in 40ul of Optimem were incubated with an equal volume of the transfection mix for 2h at 3% O2, 5% CO2, 37°C in Eppendorf tubes whose caps had had been punctured with a needle to allow gas exchange. Two hours after transfection, three volumes of fresh growth medium were added and cells were plated at 10k/cm2 in Matrigel coated wells containing growth media. Two days upon transfection wells were processed for immunostaining or RNA collected with Tryzol as above. Details on immunostaining, RT-qPCR ans Western Blot are described in Supplemental Methods.

Lentivirus transduction for gain and loss of function experiments

For GOF asays, in-lab made lentiviral viruses (control (PLVX-CAG-P2A-mCherry) and Foxc1-mCherry (PLVX-CAG-Foxc1-P2A-mCherry), CAG promoter) and viruses produced by VectorBuilder

(https://en.vectorbuilder.com/) (control (pLVX-EF1A>mCherry), Foxc1-mCherry (pLVX-EF1A>mFoxc1-T2A-mCherry), Creb3l1-mCherry (pLVX-EF1A>mCreb3l1-T2A-mCherry), EF1a promoter) were used. T2A or P2A causes co-translational cleavage of the encoded polypeptide (Supplementary Table 12). GOF assays of FOXC1 with in-lab or vector builder made viruses were used interchangeably as they gave comparable results. For LOF assays, three different Foxc1-shRNA vectors were tested with identical results (U6 promoter for shRNA and hPGK for mCherry reporter).

Freshly isolated satellite cells from *Tg:Pax7-nGFP* mice were plated in matrigel coated wells, cultured overnight and transduced at an MOI (multiplicity of infection) of 100 in 45μl (for 96 well plates) or 125μl (for 48 well plates) of MuSC media containing 5 μg/ml of polybrene. After 4h incubation at 37°C, cells were washed three times with media and cultured for 4 more days in GM prior to fixation for immunostaining, protein or RNA collection, or re-sorting of mCherry+ when needed.

Image analysis

For cells grown on 96 wells, images from the Opera Phenix high-content microscope were quantified using Harmony software and a semi-automated pipeline. Nuclei were detected based on Hoechst signal and mean intensity of fluorescence were automatically quantified on the nuclear region for nuclear markers. Number of nuclei positive for a certain nuclear marker were scored on a manually defined threshold. For cells grown on IBIDI 8 well plates, czi images were manually quantified in a blinded manner using the point toll counter in Fiji (Schindelin et al., 2012) or using the TrackMate7 pipeline (Ershov et al., 2022).

Immunostaining on ECM markers on cells were scanned using either the Opera Phoenix high-content microscope (Perkin Elmer) or Zeiss LSM800 microscope with ZEN software. Imaging of tissue sections was done on a Zeiss LSM800 microscope or a Ti2E Spinning disk (Nikon).

The fusion index was calculated as the fraction of nuclei contained within MF20+ myotubes, which had two or more nuclei, as compared to the number of total nuclei within each image.

Figures were assembled in Adobe Photoshop, Illustrator and InDesign (Adobe Systems).

Time lapse microscopy

MuSC were plated on a microscopy culture chamber (IBIDI, 80826) or 96 wells of TC-Treated Black μCLEAR plates (Greiner Bio-One 655090) and cultured in growth media. The plate was incubated at 37°C, 5% CO_2, and 3% O_2 (Zeiss, Pecon). A Zeiss Observer.Z1 connected to a Plan-Apochromat 20x/0.8 M27 objective and Hamamatsu Orca Flash 4 camera piloted with Zen (Zeiss) was used. After activation for 3 days *in vitro*, EOM and TA cells were imaged every 12 min for ~48h. Individual cells were tracked and tdTOM intensity was scored at selected time points. Tracking of *Myog*^{tdTom} cells was performed using the Manual Tracking feature of the TrackMate plug-in (Tinevez et al., 2017) in Fiji.

For lentivirus live imaging experiments, detection of total cell numbers and mCherry positive cells was done with a custom-made pipeline. To detect cell contours from the bright field images, we retrained the « livecell » model of CellPose with CellPose 2.0 (Pachitariu and Stringer, 2022). The retraining dataset was created from small crops of the full data with low density and high density regions and the different

cell phenotypes. To homogenize the data, preprocessing of the bright field chanel was applied to all the data: we enhanced the contrast locally with CLAHE (Contrast Limited Adaptive Histogram Equalization) in Fiji (with a blocksize of 127, default parameters) and normalized the intensity (for each frame). To assess which cells were infected by the virus (mCherry+), we measured the mean mCherry fluorescent intensity in each cell normalised by the local mean fluorescent intensity in the well (by averaging the fluorescent intensity with a radius around 300 µm). This allowed to compensate for differences in illumination even within the same acquisition but can slightly under-estimate the relative intensity of cells in very dense region. Finally, the mCherry intensity chanel was thresholded after a background removal with Fiji Triangle threshold method calculated with the histrogram of the 4 time frames together.
The retrained models were then runned on the full data (cropped regions or full wells) to detect the cell contours through the Fiji plugin Trackmate-CellPose (Ershov et al., 2022) which allowed us to directly access measurements of the cells (« spots » table in TrackMate).

Data analysis and statistics

Data analysis, statistics and visualisations were performed using Prism (Graphpad Software) or using R (Team, 2014) and the package ggplot2 (Wickham, 2009). Tests are described on Figure legends.
Information related to microarray data analysis and sc-RNAseq of DMD rat EOM are described in Supplemental Methods.

scRNAseq data generation

MuSCs were isolated on BD FACSAria™ III based on GFP fluorescence and cell viability from *Tg:Pax7-nGFP mice* (Sambasivan et al., 2009). Quiescent MuSCs were manually counted using a hemocytometer and immediately processed for scRNA-seq. For activated samples, MuSCs were cultured *in vitro* as described above for four days. Activated MuSCs were subsequently trypsinized and washed in DMEM/F12 2% FBS. Live cells were re-sorted, manually counted using a hemocytometer and processed for scRNA-seq.
Prior to scRNAseq, RNA integrity was assessed using Agilent Bioanalyzer 2100 to validate the isolation protocol (RIN>8 was considered acceptable). 10X Genomics Chromium microfluidic chips were loaded with around 9000 and cDNA libraries were generated following manufacturer's protocol. Concentrations and fragment sizes were determined using Agilent Bioanalyzer and Invitrogen Qubit. cDNA libraries were sequenced using NextSeq 500 and High Output v2.5 (75 cycles) kits. Count matrices were subsequently generated following 10X Genomics Cell Ranger pipeline.
Following normalisation and quality control, we obtained an average of 5792 ± 1415 cells/condition.

Seurat preprocessing

scRNAseq datasets were processed using Seurat (https://satijalab.org/seurat/) (Butler et al., 2018). Cells with more than 10% of mitochondrial gene fraction were discarded. 4000-5000 genes were detected on average across all 4 datasets. Dimensionality reduction and UMAPs were generated following Seurat workflow. The top 100 DEGs were determined using Seurat "FindAllMarkers" function with default parameters. When processed independently (scvelo), the datasets were first regressed on

cell cycle genes, mitochondrial fraction, number of genes, number of UMI following Seurat dedicated vignette, and doublets were removed using DoubletFinder v3 (McGinnis et al., 2019). A "StressIndex" score was generated for each cell based on the list of stress genes previously reported (Machado et al., 2021) using the “AddModule” Seurat function. 94 out of 98 genes were detected in the combined datasets. UMAPs were generated after 1. StressIndex regression, and 2. after complete removal of the detected stress genes from the gene expression matrix before normalization. In both cases, the overall aspect of the UMAP did not change significantly (**Figure S5**). Although immeasurable confounding effects of cell stress following isolation cannot be ruled out, we reasoned that our datasets did not show a significant effect of stress with respect to the conclusions of our study.

Matrisome analysis

After subsetting for the features of the Matrisome database (Naba et al., 2015) present in our single-cell dataset, the matrisome score was calculated by assessing the overall expression of its constituents using the "AddModuleScore" function from Seurat (Butler et al., 2018).

RNA velocity and driver genes

Scvelo was used to calculate RNA velocities (Bergen et al., 2020). Unspliced and spliced transcript matrices were generated using velocyto (Manno et al., 2018) command line function. Seurat-generated filtering, annotations and cell-embeddings (UMAP, tSNE, PCA) were then added to the outputted objects. These datasets were then processed following scvelo online guide and documentation. Velocity was calculated based on the dynamical model (using *scv.tl.recover_dynamics(adata)*, and *scv.tl.velocity(adata, mode='dynamical')*) and differential kinetics calculations were added to the model (using *scv.tl.velocity(adata, diff_kinetics=True)*). Specific driver genes were identified by determining the top likelihood genes in the selected cluster. The lists of top 100 drivers for EOM and TA progenitors are given in Supplemental Tables 10 and 11.

Gene regulatory network inference and transcription factor modules

Gene regulatory networks were inferred using pySCENIC (Aibar et al., 2017; Sande et al., 2020). This algorithm regroups sets of correlated genes into regulons (i.e. a transcription factor and its targets) based on binding motifs and co-expression patterns. The top 35 regulons for each cluster was determined using scanpy "scanpy.tl.rank_genes_groups" function (method=t-test). Note that this function can yield less than 35 results depending on the cluster. UMAP and heatmap were generated using regulon AUC matrix (Area Under Curve) which refers to the activity level of each regulon in a given cell. Visualizations were performed using scanpy (Wolf et al., 2018). The outputted list of each regulon and their targets was subsequently used to create a transcription factor network. To do so, only genes that are regulons themselves were kept. This results in a visual representation where each node is an active transcription factor and each edge is an inferred regulation between 2 transcription factors. When placed in a force-directed environment, these nodes aggregate based on the number of shared edges. This operation greatly reduced the number of genes involved, while highlighting co-regulating transcriptional modules. Visualization of this network was performed in a force-directed graph using

Gephi “Force-Atlas2” algorithm (https://gephi.org/). Of note, a force-directed graph is a type of visualization technique where nodes are positioned based on the principles of physics that assign forces among the set of edges and the set of nodes. Spring like attractive forces are used to attract pairs of edges towards each other (connected nodes) while repulsive forces, like those of electrically charged particles, are used to separate all pairs of nodes. In the equilibrium state for this system, the edges tend to have uniform length (because of the spring forces), and nodes that are not connected by an edge tend to be drawn further apart (because of the electrical repulsion).

Gene ontology analysis

Gene ontology analyses were performed on top 100 markers (obtained from Seurat function FindAllMarkers) or on top 100 driver genes (obtained from scvelo), using Cluego (Bindea et al., 2009). “GO Molecular Pathway”, and “REACTOME pathways” were used independently to identify common and unique pathways involved in each dataset. In all analyses, an enrichment/depletion two-sided hypergeometric test was performed and p-values were corrected using the Bonferroni step down method. Only the pathways with a p-value lower than 0.05 were displayed.

Literature scores

The scores for SMMCs (Giordani et al., 2019), FAPs (Oprescu et al., 2020), myotendinous junction B myonuclei (Kim et al., 2020), Twist2+ population(Liu et al., 2017), fetal MuSCs (Tierney et al., 2016), developing limb connective tissues (Lima et al., 2021) and the human skeletal muscle mesenchyme (Xi et al., 2020) were calculated by assessing the overall expression of the markers of each population (Supplemental Table 5) using the "AddModuleScore" function from Seurat (Butler et al., 2018).

Code availability and Data availability

The code that was used to generate the TF network is available at this address: https://github.com/TajbakhshLab/TFnetwork. scRNAseq datasets are available in open access on DRYAD at the following address: (to be updated if manuscript accepted). Raw data scRNAseq sequencing data have been deposited in the NCBI Gene Expression Omnibus database with the accession code: GSE244964.

Acknowledgements

We acknowledge funding support from the Institut Pasteur, Agence Nationale de la Recerche (Laboratoire d’Exellence Revive, Investissement d’Avenir; ANR-10-LABX-73 to ST and ANR-21-CE13-0005 MUSE to GC), Association Française contre les Myopathies (Grant #20510 to ST and #23201 to GC), and the Centre National de la Recherche Scientifique. M.B.D. was supported by a grant from Laboratoire d’Excellence Revive and La Ligue Contre le Cancer. We gratefully acknowledge the Genomic Patform (Inserm U1016-CNRS UMRS 8104 - Université de Paris Cité) at Institut Cochin, the UtechS Photonic BioImaging (Imagopole), C2RT, Institut Pasteur, supported by the French National Research Agency (France BioImaging; ANR-10–INSB–04; Investments for the Future) and the Center for Translational Science (CRT)-Cytometry and Biomarkers Unit of Technology and Service (CB

UTechS) at Institut Pasteur for support in conducting this study. We warmly thank Pierre Henri Comere for assistance with cell sorting and Marion Louveaux for establishment of the initial image analysis pipeline.

Author contributions

MBD, GC, and ST conceived the study. DDG, MM, MDB, PTL and GC performed experiments. PTL, SG, MK and BE contributed to *in vitro* experiments and image acquisition. AG, MBD and DDG performed sc-RNAseq. AG and MBD run the bioinformatic analysis with help from SM and VL. JYT and GL performed image analysis. AG, MBD and GC wrote the manuscript with input from DDG, MM and ST. GC and ST provided funding.

REFERENCES

Ahmad, S., Jan, A. T., Baig, M. H., Lee, E. J. and Choi, I. (2017). Matrix gla protein: An extracellular matrix protein regulates myostatin expression in the muscle developmental program. *Life Sci* **172**, 55–63.

Aibar, S., González-Blas, C. B., Moerman, T., Huynh-Thu, V. A. A., Imrichova, H., Hulselmans, G., Rambow, F., Marine, J.-C. C., Geurts, P., Aerts, J., et al. (2017). SCENIC: single-cell regulatory network inference and clustering. *Nature methods* **14**, 1083–1086.

Alexakis, C., Partridge, T. and Bou-Gharios, G. (2007). Implication of the satellite cell in dystrophic muscle fibrosis: a self-perpetuating mechanism of collagen overproduction. *Am J Physiol-cell Ph* **293**, C661–C669.

Almada, A. E., Horwitz, N., Price, F. D., Gonzalez, A. E., Ko, M., Bolukbasi, O. V., Messemer, K. A., Chen, S., Sinha, M., Rubin, L. L., et al. (2021). FOS licenses early events in stem cell activation driving skeletal muscle regeneration. *Cell Reports* **34**, 108656.

Andrés, V. and Walsh, K. (1996). Myogenin expression, cell cycle withdrawal, and phenotypic differentiation are temporally separable events that precede cell fusion upon myogenesis. *J Cell Biology* **132**, 657–66.

Artico, L. L., Laranjeira, Angelo Brunelli Albertoni, Campos, Livia Weijenborg, Correa, J. R., Zenatti, P. P., Carvalheira, J. B. C., Brambilla, S. R., Nowill, A. E., Brandalise, S. R. and Junes, J. A. (2021). Physiologic IGFBP7 levels prolong IGF1R activation in acute lymphoblastic leukemia. *Blood advances* **18**,.

Baghdadi, M. B., Castel, D., Machado, L., Fukada, S., Birk, D. E., Relaix, F., Tajbakhsh, S. and Mourikis, P. (2018). Reciprocal signalling by Notch–Collagen V–CALCR retains muscle stem cells in their niche. *Nature* **557**, 714–718.

Barruet, E., Garcia, S. M., Striedinger, K., Wu, J., Lee, S., Byrnes, L., Wong, A., Xuefeng, S., Tamaki, S., Brack, A. S., et al. (2020). Functionally heterogeneous human satellite cells identified by single cell RNA sequencing. *Elife* **9**, e51576.

Benavente-Diaz, M., Comai, G., Girolamo, D. D., Langa, F. and Tajbakhsh, S. (2021). Dynamics of myogenic differentiation using a novel Myogenin knock-in reporter mouse. *Skelet Muscle* **11**, 5.

Bentzinger, F. C., Wang, Y., von Maltzahn, J., Soleimani, V. D., Yin, H. and Rudnicki, M. A. (2013). Fibronectin Regulates Wnt7a Signaling and Satellite Cell Expansion. *Cell Stem Cell* **12**, 75–87.

Bergen, V., Lange, M., Peidli, S., Wolf, F. A. and Theis, F. J. (2020). Generalizing RNA velocity to transient cell states through dynamical modeling. *Nat Biotechnol* 1–7.

Bindea, G., Mlecnik, B., Hackl, H., Charoentong, P., Tosolini, M., Kirilovsky, A., Fridman, W.-H., Pagès, F., Trajanoski, Z. and Galon, J. (2009). ClueGO: a Cytoscape plug-in to decipher functionally grouped gene ontology and pathway annotation networks. *Bioinformatics* **25**, 1091–1093.

Briggs, D. and Morgan, J. E. (2013). Recent progress in satellite cell/myoblast engraftment – relevance for therapy. *FEBS Journal* **280**, 4281–4293.

Brink, S. C. van den, Sage, F., Vértesy, Á., Spanjaard, B., Peterson-Maduro, J., Baron, C. S., Robin, C. and Oudenaarden, A. van (2017). Single-cell sequencing reveals dissociation-induced gene expression in tissue subpopulations. *Nat Methods* **14**, 935–936.

Brohmann, H., Jagla, K. and Birchmeier, C. (2000). The role of Lbx1 in migration of muscle precursor cells. *Development* **127**, 437–445.

Butler, A., Hoffman, P., Smibert, P., Papalexi, E. and Satija, R. (2018). Integrating single-cell transcriptomic data across different conditions, technologies, and species. *Nat Biotechnol* **36**, 411–420.

Cappellari, O., Benedetti, S., Innocenzi, A., Tedesco, F. S., Moreno-Fortuny, A., Ugarte, G., Lampugnani, M. G., Messina, G. and Cossu, G. (2013). Dll4 and PDGF-BB Convert Committed Skeletal Myoblasts to Pericytes without Erasing Their Myogenic Memory. *Dev Cell* **24**, 586–599.

Chakkalakal, J. V., Christensen, J., Xiang, W., Tierney, M. T., Boscolo, F. S., Sacco, A. and Brack, A. S. (2014). Early forming label-retaining muscle stem cells require p27kip1 for maintenance of the primitive state. *Development* **141**, 1649–1659.

Charville, G. W., Cheung, T. H., Yoo, B., Santos, P. J., Lee, G. K., Shrager, J. B. and Rando, T. A. (2015). Ex Vivo Expansion and In Vivo Self-Renewal of Human Muscle Stem Cells. *Stem Cell Reports* **5**, 621–632.

Chen, Z., Li, L., Wu, W., Liu, Z., Huang, Y., Yang, L., Luo, Q., Chen, J., Hou, Y. and Song, G. (2020). Exercise protects proliferative muscle satellite cells against exhaustion via the Igfbp7-Akt-mTOR axis. *Theranostics* **10**, 6448–6466.

Cho, W. J., Kim, E. J., Lee, S. J., Kim, H. D., Shin, H. J. and Lim, W. K. (2000). Involvement of SPARC in in Vitro Differentiation of Skeletal Myoblasts. *Biochem Bioph Res Co* **271**, 630–634.

Clemmons, D. R. (1997). Insulin-like growth factor binding proteins and their role in controlling IGF actions. *Cytokine Growth Factor Rev.* **8**, 45–62.

Contreras, O., Córdova-Casanova, A. and Brandan, E. (2021). PDGF-PDGFR network differentially regulates the fate, migration, proliferation, and cell cycle progression of myogenic cells. *Cell Signal* **84**, 110036.

Dell'Orso, S., Juan, A. H., Ko, K.-D., Naz, F., Perovanovic, J., Gutierrez-Cruz, G., Feng, X. and Sartorelli, V. (2019). Single cell analysis of adult mouse skeletal muscle stem cells in homeostatic and regenerative conditions. *Development* **146**, dev174177.

Diehl, A. G., Zareparsi, S., Qian, M., Khanna, R., Angeles, R. and Gage, P. J. (2006). Extraocular Muscle Morphogenesis and Gene Expression Are Regulated by Pitx2 Gene Dose. *Investigative Ophthalmology & Visual Science* **47**, 1785–1793.

Dionyssiou, M. G., Salma, J., Bevzyuk, M., Wales, S., Zakharyan, L. and McDermott, J. C. (2013). Krüppel-like factor 6 (KLF6) promotes cell proliferation in skeletal myoblasts in response to TGFβ/Smad3 signaling. *Skelet Muscle* **3**, 7.

Dulauroy, S., Carlo, S. E., Langa, F., Eberl, G. and Peduto, L. (2012). Lineage tracing and genetic ablation of ADAM12+ perivascular cells identify a major source of profibrotic cells during acute tissue injury. *Nature Medicine* **18**, 1262–1270.

Dumont, N. A., Wang, Y. X., Maltzahn, J. von, Pasut, A., Bentzinger, C. F., Brun, C. E. and Rudnicki, M. A. (2015). Dystrophin expression in muscle stem cells regulates their polarity and asymmetric division. *Nat Med* **21**, 1455–1463.

El-Magd, M. A., Abdelfattah-Hassan, A., Elsisy, R. A., Hawsawi, Y. M., Oyouni, A. A., Al-Amer, O. M. and El-Shetry, E. S. (2021). Expression and function of Ebf1 gene during chondrogenesis in chick embryo limb buds. *Gene* **803**, 145895.

Emery, A. E. (2002). The muscular dystrophies. *Lancet* **359**, 687–695.

Engert, J. C., Berglund, E. B. and Rosenthal, N. (1996). Proliferation precedes differentiation in IGF-I-stimulated myogenesis. *J. cell Biol.* **135**, 431–440.

Ershov, D., Phan, M.-S., Pylvänäinen, J. W., Rigaud, S. U., Blanc, L. L., Charles-Orszag, A., Conway, J. R. W., Laine, R. F., Roy, N. H., Bonazzi, D., et al. (2022). TrackMate 7: integrating state-of-the-art segmentation algorithms into tracking pipelines. *Nat. Methods* **19**, 829–832.

Evano, B. and Tajbakhsh, S. (2018). Skeletal muscle stem cells in comfort and stress. *npj Regenerative Medicine* **3**, 24.

Evano, B., Gill, D., Hernando-Herraez, I., Comai, G., Stubbs, T. M., Commere, P.-H., Reik, W. and Tajbakhsh, S. (2020). Transcriptome and epigenome diversity and plasticity of muscle stem cells following transplantation. *Plos Genet* **16**, e1009022.

Faggi, F., Chiarelli, N., Colombi, M., Mitola, S., Ronca, R., Madaro, L., Bouche, M., Poliani, P. L., Vezzoli, M., Longhena, F., et al. (2015). Cavin-1 and Caveolin-1 are both required to support cell proliferation, migration and anchorage-independent cell growth in rhabdomyosarcoma. *Lab Invest* **95**, 585–602.

Formicola, L., Marazzi, G. and Sassoon, D. A. (2014). The extraocular muscle stem cell niche is resistant to ageing and disease. *Front Aging Neurosci* **6**, 328.

Fukada, S., Uezumi, A., Ikemoto, M., Masuda, S., Segawa, M., Tanimura, N., Yamamoto, H., Miyagoe-Suzuki, Y. and Takeda, S. (2007). Molecular Signature of Quiescent Satellite Cells in Adult Skeletal Muscle. *Stem Cells* **25**, 2448–2459.

Gage, P. J., Suh, H. and Camper, S. A. (1999). Dosage requirement of Pitx2 for development of multiple organs. *Development* **126**, 4643–4651.

García, I. A., Demichelis, V. T., Viale, D. L., Giusto, P. D., Ezhova, Y., Polishchuk, R. S., Sampieri, L., Martinez, H., Sztul, E. and Alvarez, C. (2017). CREB3L1-mediated functional and structural adaptation of the secretory pathway in hormone-stimulated thyroid cells. *J Cell Sci* **130**, 4155–4167.

Gattazzo, F., Laurent, B., Relaix, F., Rouard, H. and Didier, N. (2020a). Distinct Phases of Postnatal Skeletal Muscle Growth Govern the Progressive Establishment of Muscle Stem Cell Quiescence. *Stem Cell Rep*.

Gattazzo, F., Laurent, B., Relaix, F., Rouard, H. and Didier, N. (2020b). Distinct Phases of Postnatal Skeletal Muscle Growth Govern the Progressive Establishment of Muscle Stem Cell Quiescence. *Stem Cell Rep*.

Gaut, L., Robert, N., Delalande, A., Bonnin, M.-A., Pichon, C. and Duprez, D. (2016). EGR1 Regulates Transcription Downstream of Mechanical Signals during Tendon Formation and Healing. *Plos One* **11**, e0166237.

Gayraud-Morel, B., Chrétien, F., Jory, A., Sambasivan, R., Negroni, E., Flamant, P., Soubigou, G., Coppée, J.-Y., Santo, J., Cumano, A., et al. (2012). Myf5 haploinsufficiency reveals distinct cell fate potentials for adult skeletal muscle stem cells. *Journal of Cell Science* **125**, 1738–1749.

Gayraud-Morel, B., Pala, F., Sakai, H. and Tajbakhsh, S. (2017). Isolation of Muscle Stem Cells from Mouse Skeletal Muscle. *Methods Mol Biology Clifton N J* **1556**, 23–39.

Gerli, M., Moyle, L., Benedetti, S., Ferrari, G., Ucuncu, E., Ragazzi, M., Constantinou, C., Louca, I., Sakai, H., Ala, P., et al. (2019). Combined Notch and PDGF Signaling Enhances Migration and Expression of Stem Cell Markers while Inducing Perivascular Cell Features in Muscle Satellite Cells. *Stem Cell Rep* **12**, 461–473.

Giordani, L., He, G. J., Negroni, E., Sakai, H., Law, J., Siu, M. M., Wan, R., Corneau, A., Tajbakhsh, S., Cheung, T. H., et al. (2019). High-Dimensional Single-Cell Cartography Reveals Novel Skeletal Muscle-Resident Cell Populations. *Mol Cell* **74**, 609-621.e6.

Gnocchi, V. F., White, R. B., Ono, Y., Ellis, J. A. and Zammit, P. S. (2009). Further Characterisation of the Molecular Signature of Quiescent and Activated Mouse Muscle Satellite Cells. *Plos One* **4**, e5205.

Gonçalves, P. R., Nascimento, L. D., Gerlach, R. F., Rodrigues, K. E. and Prado, A. F. (2022). Matrix Metalloproteinase 2 as a Pharmacological Target in Heart Failure. *Pharm* **15**, 920.

Gopalakrishnan, S., Comai, G., Sambasivan, R., Francou, A., Kelly, R. G. and Tajbakhsh, S. (2015). A Cranial Mesoderm Origin for Esophagus Striated Muscles. *Developmental Cell* **34**, 694–704.

Grimaldi, A. and Tajbakhsh, S. (2021). Diversity in cranial muscles: Origins and developmental programs. *Curr Opin Cell Biol* **73**, 110–116.

Grimaldi, A., Comai, G., Mella, S. and Tajbakhsh, S. (2022). Identification of bipotent progenitors that give rise to myogenic and connective tissues in mouse. *Elife* **11**, e70235.

Gross, M., Moran-Rivard, L., Velasquez, T., Nakatsu, M., Jagla, K. and Goulding, M. (2000). Lbx1 is required for muscle precursor migration along a lateral pathway into the limb. *Development (Cambridge, England)* **127**, 413–24.

Günther, S., Mielcarek, M., Krüger, M. and Braun, T. (2004). VITO-1 is an essential cofactor of TEF1-dependent muscle-specific gene regulation. *Nucleic Acids Res* **32**, 791–802.

Guo, K., Wang, J., Andrés, V., Smith, R. C. and Walsh, K. (1995). MyoD-induced expression of p21 inhibits cyclin-dependent kinase activity upon myocyte terminal differentiation. *Mol Cell Biol* **15**, 3823–9.

György, I., Boller, S., Nechanitzky, R., Mandel, E., Pott, S., Liu, E. and Grosschedl, R. (2012). Transcription factor Ebf1 regulates differentiation stage-specific signaling, proliferation, and survival of B cells. *Gene Dev* **26**, 668–682.

Haldar, M., Hancock, J. D., Coffin, C. M., Lessnick, S. L. and Capecchi, M. R. (2007). A Conditional Mouse Model of Synovial Sarcoma: Insights into a Myogenic Origin. *Cancer Cell* **11**, 375–388.

Hamilton, T. G., Klinghoffer, R. A., Corrin, P. D. and Soriano, P. (2003). Evolutionary Divergence of Platelet-Derived Growth Factor Alpha Receptor Signaling Mechanisms. *Mol. Cell. Biol.* **23**, 4013–4025.

Han, B., Bhowmick, N., Qu, Y., Chung, S., Giuliano, A. E. and Cui, X. (2017). FOXC1: an emerging marker and therapeutic target for cancer. *Oncogene* **36**, 3957–3963.

Harel, I., Nathan, E., Tirosh-Finkel, L., Zigdon, H., Guimarães-Camboa, N., Evans, S. M. and Tzahor, E. (2009). Distinct Origins and Genetic Programs of Head Muscle Satellite Cells. *Dev Cell* **16**, 822–832.

Havis, E. and Duprez, D. (2020). EGR1 Transcription Factor is a Multifaceted Regulator of Matrix Production in Tendons and Other Connective Tissues. *Int J Mol Sci* **21**, 1664.

Hebert, S. L., Daniel, M. L. and McLoon, L. K. (2013). The Role of Pitx2 in Maintaining the Phenotype of Myogenic Precursor Cells in the Extraocular Muscles. *PLoS ONE* **8**, e58405.

Hellström, M., Kalén, M., Lindahl, P., Abramsson, A. and Betsholtz, C. (1999). Role of PDGF-B and PDGFR-beta in recruitment of vascular smooth muscle cells and pericytes during embryonic blood vessel formation in the mouse. *Dev Camb Engl* **126**, 3047–55.

Hernando-Herraez, I., Evano, B., Stubbs, T., Commere, P.-H., Bonder, M. J., Clark, S., Andrews, S., Tajbakhsh, S. and Reik, W. (2019). Ageing affects DNA methylation drift and transcriptional cell-to-cell variability in mouse muscle stem cells. *Nat Commun* **10**, 4361.

Honda, M., Hidaka, K., Fukada, S., Sugawa, R., Shirai, M., Ikawa, M. and Morisaki, T. (2017). Vestigial-like 2 contributes to normal muscle fiber type distribution in mice. *Sci Rep-uk* **7**, 7168.

Ikemoto, M., Fukada, S., Uezumi, A., Masuda, S., Miyoshi, H., Yamamoto, H., Wada, M. R., Masubuchi, N., Miyagoe-Suzuki, Y. and Takeda, S. (2007). Autologous Transplantation of SM/C-2.6+ Satellite Cells

Transduced with Micro-dystrophin CS1 cDNA by Lentiviral Vector into mdx Mice. *Molecular Therapy* **15**, 2178–2185.

Ishii, K., Sakurai, H., Suzuki, N., Mabuchi, Y., Sekiya, I., Sekiguchi, K. and Akazawa, C. (2018). Recapitulation of Extracellular LAMININ Environment Maintains Stemness of Satellite Cells In Vitro. *Stem Cell Rep* **10**, 568–582.

Jen, Y., Weintraub, H. and Benezra, R. (1992). Overexpression of Id protein inhibits the muscle differentiation program: in vivo association of Id with E2A proteins. *Gene Dev* **6**, 1466–1479.

Jimenez, M. A., Åkerblad, P., Sigvardsson, M. and Rosen, E. D. (2007). Critical Role for Ebf1 and Ebf2 in the Adipogenic Transcriptional Cascade. *Mol Cell Biol* **27**, 743–757.

Jin, L., Shen, F., Weinfeld, M. and Sergi, C. (2020). Insulin Growth Factor Binding Protein 7 (IGFBP7)-Related Cancer and IGFBP3 and IGFBP7 Crosstalk. *Frontiers Oncol* **10**, 727.

Jing, Y., Jin, Y., Wang, Y., Chen, S., Zhang, X., Song, Y., Wang, Z., Pu, Y., Ni, Y. and Hu, Q. (2019). SPARC promotes the proliferation and metastasis of oral squamous cell carcinoma by PI3K/AKT/PDGFB/PDGFRβ axis. *J Cell Physiol* **234**, 15581–15593.

Joe, A. W. B., Yi, L., Natarajan, A., Grand, F. L., So, L., Wang, J., Rudnicki, M. A. and Rossi, F. M. V. (2010). Muscle injury activates resident fibro/adipogenic progenitors that facilitate myogenesis. *Nat Cell Biol* **12**, 153–163.

Kallestad, K. M., Hebert, S. L., McDonald, A. A., Daniel, M. L., Cu, S. R. and McLoon, L. K. (2011). Sparing of extraocular muscle in aging and muscular dystrophies: A myogenic precursor cell hypothesis. *Experimental Cell Research* **317**, 873–885.

Kelly, R. G., Jerome-Majewska, L. A. and Papaioannou, V. E. (2004). The del22q11.2 candidate gene Tbx1 regulates branchiomeric myogenesis. *Human Molecular Genetics* **13**, 2829–2840.

Kida, Y. and Yamaguchi, I. (2022). The vascular protective effect of matrix Gla protein during kidney injury. *Frontiers Mol Medicine* **2**, 970744.

Kim, M., Franke, V., Brandt, B., Lowenstein, E. D., Schöwel, V., Spuler, S., Akalin, A. and Birchmeier, C. (2020). Single-nucleus transcriptomics reveals functional compartmentalization in syncytial skeletal muscle cells. *Nat Commun* **11**, 6375.

Kotsaris, G., Qazi, T. H., Bucher, C. H., Zahid, H., Pöhle-Kronawitter, S., Ugorets, V., Jarassier, W., Börno, S., Timmermann, B., Giesecke-Thiel, C., et al. (2023). Odd skipped-related 1 controls the pro-regenerative response of fibro-adipogenic progenitors. *npj Regen. Med.* **8**, 19.

Kühl, U., Öcalan, M., Timpl, R., Mayne, R., Hay, E. and Mark, K. von der (1984). Role of muscle fibroblasts in the deposition of type-IV collagen in the basal lamina of myotubes. *Differentiation* **28**, 164–172.

Kumar, D., Shadrach, J. L., Wagers, A. J. and Lassar, A. B. (2009). Id3 Is a Direct Transcriptional Target of Pax7 in Quiescent Satellite Cells. *Mol Biol Cell* **20**, 3170–3177.

Lagha, M., Brunelli, S., Messina, G., Cumano, A., Kume, T., Relaix, F. and Buckingham, M. E. (2009). Pax3:Foxc2 Reciprocal Repression in the Somite Modulates Muscular versus Vascular Cell Fate Choice in Multipotent Progenitors. *Dev Cell* **17**, 892–899.

Laumonier, T., Bermont, F., Hoffmeyer, P., Kindler, V. and Menetrey, J. (2017). Human myogenic reserve cells are quiescent stem cells that contribute to muscle regeneration after intramuscular transplantation in immunodeficient mice. *Sci Rep-uk* **7**, 3462.

Lay, K., Kume, T. and Fuchs, E. (2016). FOXC1 maintains the hair follicle stem cell niche and governs stem cell quiescence to preserve long-term tissue-regenerating potential. *Proc. Natl. Acad. Sci.* **113**, E1506–E1515.

Levéen, P., Pekny, M., Gebre-Medhin, S., Swolin, B., Larsson, E. and Betsholtz, C. (1994). Mice deficient for PDGF B show renal, cardiovascular, and hematological abnormalities. *Gene Dev* **8**, 1875–1887.

L'honoré, A., Commère, P.-H., Negroni, E., Pallafacchina, G., Friguet, B., Drouin, J., Buckingham, M. and Montarras, D. (2018). The role of Pitx2 and Pitx3 in muscle stem cells gives new insights into P38α MAP kinase and redox regulation of muscle regeneration. *eLife* **7**, e32991.

Li, X., Wei, R., Wang, M., Ma, L., Zhang, Z., Chen, L., Guo, Q., Guo, S., Zhu, S., Zhang, S., et al. (2020). MGP Promotes Colon Cancer Proliferation by Activating the NF-κB Pathway through Upregulation of the Calcium Signaling Pathway. *Mol Ther - Oncolytics* **17**, 371–383.

Lima, J. E. de, Blavet, C., Bonnin, M.-A., Hirsinger, E., Comai, G., Yvernogeau, L., Delfini, M.-C., Bellenger, L., Mella, S., Nassari, S., et al. (2021). Unexpected contribution of fibroblasts to muscle lineage as a mechanism for limb muscle patterning. *Nat Commun* **12**, 3851.

Liu, L., Cheung, T. H., Charville, G. W. and Rando, T. A. (2015). Isolation of skeletal muscle stem cells by fluorescence-activated cell sorting. *Nat. Protoc.* **10**, 1612–1624.

Liu, N., Garry, G. A., Li, S., Bezprozvannaya, S., Sanchez-Ortiz, E., Chen, B., Shelton, J. M., Jaichander, P., Bassel-Duby, R. and Olson, E. N. (2017). A Twist2-dependent progenitor cell contributes to adult skeletal muscle. *Nat Cell Biol* **19**, 202–213.

Lukjanenko, L., Jung, J. M., Hegde, N., Perruisseau-Carrier, C., Migliavacca, E., Rozo, M., Karaz, S., Jacot, G., Schmidt, M., Li, L., et al. (2016). Loss of fibronectin from the aged stem cell niche affects the regenerative capacity of skeletal muscle in mice. *Nature Medicine* **22**, 897–905.

Machado, L., Lima, J. E. de, Fabre, O., Proux, C., Legendre, R., Szegedi, A., Varet, H., Ingerslev, L. R., Barrès, R., Relaix, F., et al. (2017). In Situ Fixation Redefines Quiescence and Early Activation of Skeletal Muscle Stem Cells. *Cell Reports* **21**, 1982–1993.

Machado, L., Geara, P., Camps, J., Santos, M. D., Teixeira-Clerc, F., Herck, J. V., Varet, H., Legendre, R., Pawlotsky, J.-M., Sampaolesi, M., et al. (2021). Tissue damage induces a conserved stress response that initiates quiescent muscle stem cell activation. *Cell Stem Cell*.

Madisen, L., Zwingman, T. A., Sunkin, S. M., Oh, S., Zariwala, H. A., Gu, H., Ng, L. L., Palmiter, R. D., Hawrylycz, M. J., Jones, A. R., et al. (2009). A robust and high-throughput Cre reporting and characterization system for the whole mouse brain. *Nature Neuroscience* **13**, 133–140.

Maeda, T., Chapman, D. L. and Stewart, A. F. R. (2002). Mammalian Vestigial-like 2, a Cofactor of TEF-1 and MEF2 Transcription Factors That Promotes Skeletal Muscle Differentiation*. *J Biol Chem* **277**, 48889–48898.

Manno, G. L., Soldatov, R., Zeisel, A., Braun, E., Hochgerner, H., Petukhov, V., Lidschreiber, K., Kastriti, M. E., Lönnerberg, P., Furlan, A., et al. (2018). RNA velocity of single cells. *Nature* **560**, 494–498.

Mathew, S. J., Hansen, J. M., Merrell, A. J., Murphy, M. M., Lawson, J. A., Hutcheson, D. A., Hansen, M. S., Angus-Hill, M. and Kardon, G. (2011). Connective tissue fibroblasts and Tcf4 regulate myogenesis. *Development* **138**, 371–384.

Mayeuf-Louchart, A., Montarras, D., Bodin, C., Kume, T., Vincent, S. D. and Buckingham, M. (2016). Endothelial cell specification in the somite is compromised in Pax3-positive progenitors of Foxc1/2 conditional mutants, with loss of forelimb myogenesis. *Development* **143**, 872–879.

McDavid, A., Finak, G. and Gottardo, R. (2016). The contribution of cell cycle to heterogeneity in single-cell RNA-seq data. *Nat Biotechnol* **34**, 591–593.

McGinnis, C. S., Murrow, L. M. and Gartner, Z. J. (2019). DoubletFinder: Doublet Detection in Single-Cell RNA Sequencing Data Using Artificial Nearest Neighbors. *Cell Syst* **8**, 329-337.e4.

McLoon, L. K., Vicente, A., Fitzpatrick, K. R., Lindström, M. and Domellöf, F. (2018). Composition, Architecture, and Functional Implications of the Connective Tissue Network of the Extraocular Muscles. *Investigative Ophthalmology & Visual Science* **59**, 322–329.

Melouane, A., Carbonell, A., Yoshioka, M., Puymirat, J. and St-Amand, J. (2018). Implication of SPARC in the modulation of the extracellular matrix and mitochondrial function in muscle cells. *Plos One* **13**, e0192714.

Michailovici, I., Eigler, T. and Tzahor, E. (2015). Chapter One Craniofacial Muscle Development. *Curr Top Dev Biol* **115**, 3–30.

Micheli, A. J. D., Laurilliard, E. J., Heinke, C. L., Ravichandran, H., Fraczek, P., Soueid-Baumgarten, S., Vlaminck, I., Elemento, O. and Cosgrove, B. D. (2020). Single-Cell Analysis of the Muscle Stem Cell Hierarchy Identifies Heterotypic Communication Signals Involved in Skeletal Muscle Regeneration. *Cell Reports* **30**, 3583-3595.e5.

Milet, C., Bléher, M., Allbright, K., Orgeur, M., Coulpier, F., Duprez, D. and Havis, E. (2017). Egr1 deficiency induces browning of inguinal subcutaneous white adipose tissue in mice. *Sci Rep-uk* **7**, 16153.

Montarras, D., Morgan, J., Collins, C., Relaix, F., Zaffran, S., Cumano, A., Partridge, T. and Buckingham, M. (2005). Direct Isolation of Satellite Cells for Skeletal Muscle Regeneration. *Science* **309**, 2064–2067.

Moreno, C. S. (2019). SOX4: The Unappreciated Oncogene. *Semin Cancer Biol* **67**, 57–64.

Morree, A. de, Klein, J. D. D., Gan, Q., Farup, J., Urtasun, A., Kanugovi, A., Bilen, B., Velthoven, C. T. J. van, Quarta, M. and Rando, T. A. (2019). Alternative polyadenylation of Pax3 controls muscle stem cell fate and muscle function. *Science* **366**, 734–738.

Mourikis, P., Sambasivan, R., Castel, D., Rocheteau, P., Bizzarro, V. and Tajbakhsh, S. (2012). A Critical Requirement for Notch Signaling in Maintenance of the Quiescent Skeletal Muscle Stem Cell State. *Stem Cells* **30**, 243–252.

Mu, X., Urso, M. L., Murray, K., Fu, F. and Li, Y. (2010). Relaxin Regulates MMP Expression and Promotes Satellite Cell Mobilization During Muscle Healing in Both Young and Aged Mice. *Am J Pathology* **177**, 2399–2410.

Murphy, M. M., Lawson, J. A., Mathew, S. J., Hutcheson, D. A. and Kardon, G. (2011). Satellite cells, connective tissue fibroblasts and their interactions are crucial for muscle regeneration. *Development* **138**, 3625–3637.

Naba, A., Clauser, K. R., Ding, H., Whittaker, C. A., Carr, S. A. and Hynes, R. O. (2015). The extracellular matrix: Tools and insights for the “omics” era. *Matrix Biology J Int Soc Matrix Biology* **49**, 10–24.

Noguchi, Y., Nakamura, M., Hino, N., Nogami, J., Tsuji, S., Sato, T., Zhang, L., Tsujikawa, K., Tanaka, T., Izawa, K., et al. (2019). Cell-autonomous and redundant roles of Hey1 and HeyL in muscle stem cells: HeyL requires Hes1 to bind diverse DNA sites. *Development* **146**, dev163618.

Olguin, H. C. and Olwin, B. B. (2004). Pax-7 up-regulation inhibits myogenesis and cell cycle progression in satellite cells: a potential mechanism for self-renewal. *Dev Biol* **275**, 375–388.

Ono, Y., Masuda, S., Nam, H., Benezra, R., Miyagoe-Suzuki, Y. and Takeda, S. (2012). Slow-dividing satellite cells retain long-term self-renewal ability in adult muscle. *J Cell Sci* **125**, 1309–1317.

Oprescu, S. N., Yue, F., Qiu, J., Brito, L. F. and Kuang, S. (2020). Temporal Dynamics and Heterogeneity of Cell Populations during Skeletal Muscle Regeneration. *Iscience* **23**, 100993.

Pachitariu, M. and Stringer, C. (2022). Cellpose 2.0: how to train your own model. *Nat. Methods* **19**, 1634–1641.

Pagani, F., Tratta, E., Dell'Era, P., Cominelli, M. and Poliani, P. L. (2021). EBF1 is expressed in pericytes and contributes to pericyte cell commitment. *Histochem Cell Biol* **156**, 333–347.

Randolph, M. E. and Pavlath, G. K. (2015). A muscle stem cell for every muscle: variability of satellite cell biology among different muscle groups. *Frontiers in Aging Neuroscience* **7**, 190.

Rayagiri, S., Ranaldi, D., Raven, A., Azhar, N., Lefebvre, O., Zammit, P. S. and Borycki, A.-G. (2018). Basal lamina remodeling at the skeletal muscle stem cell niche mediates stem cell self-renewal. *Nature Communications* **9**, 1075.

Relaix, F. and Zammit, P. S. (2012). Satellite cells are essential for skeletal muscle regeneration: the cell on the edge returns centre stage. *Development* **139**, 2845–2856.

Rocheteau, P., Gayraud-Morel, B., Siegl-Cachedenier, I., Blasco, M. A. and Tajbakhsh, S. (2012). A subpopulation of adult skeletal muscle stem cells retains all template DNA strands after cell division. *Cell* **148**, 112–25.

Rugowska, A., Starosta, A. and Konieczny, P. (2021). Epigenetic modifications in muscle regeneration and progression of Duchenne muscular dystrophy. *Clin Epigenetics* **13**, 13.

Sakai, H., Sato, T., Sakurai, H., Yamamoto, T., Hanaoka, K., Montarras, D. and Sehara-Fujisawa, A. (2013). Fetal Skeletal Muscle Progenitors Have Regenerative Capacity after Intramuscular Engraftment in Dystrophin Deficient Mice. *Plos One* **8**, e63016.

Sambasivan, R., Gayraud-Morel, B., Dumas, G., Cimper, C., Paisant, S., Kelly, R. G. and Tajbakhsh, S. (2009). Distinct Regulatory Cascades Govern Extraocular and Pharyngeal Arch Muscle Progenitor Cell Fates. *Developmental Cell* **16**, 810–821.

Sambasivan, R., Kuratani, S. and Tajbakhsh, S. (2011). An eye on the head: the development and evolution of craniofacial muscles. *Development* **138**, 2401–15.

Sampath, S. C., Sampath, S. C. and Millay, D. P. (2018). Myoblast fusion confusion: the resolution begins. *Skeletal Muscle* **8**, 3.

Sampieri, L., Giusto, P. D. and Alvarez, C. (2019). CREB3 Transcription Factors: ER-Golgi Stress Transducers as Hubs for Cellular Homeostasis. *Frontiers Cell Dev Biology* **7**, 123.

Sande, B. V. de, Flerin, C., Davie, K., Waegeneer, M. D., Hulselmans, G., Aibar, S., Seurinck, R., Saelens, W., Cannoodt, R., Rouchon, Q., et al. (2020). A scalable SCENIC workflow for single-cell gene regulatory network analysis. *Nat Protoc* 1–30.

Scaramozza, A., Park, D., Kollu, S., Beerman, I., Sun, X., Rossi, D. J., Lin, C. P., Scadden, D. T., Crist, C. and Brack, A. S. (2019). Lineage Tracing Reveals a Subset of Reserve Muscle Stem Cells Capable of Clonal Expansion under Stress. *Cell Stem Cell* **24**, 944-957.e5.

Schindelin, J., Arganda-Carreras, I., Frise, E., Kaynig, V., Longair, M., Pietzsch, T., Preibisch, S., Rueden, C., Saalfeld, S., Schmid, B., et al. (2012). Fiji: an open-source platform for biological-image analysis. *Nat Methods* **9**, 676–682.

Shao, X. and Wei, X. (2018). FOXP1 enhances fibrosis via activating Wnt/β-catenin signaling pathway in endometriosis. *Am J Transl Res* **10**, 3610–3618.

Smith, R. S., Zabaleta, A., Kume, T., Savinova, O. V., Kidson, S. H., Martin, J. E., Nishimura, D. Y., Alward, W. L. M., Hogan, B. L. M. and John, S. W. M. (2000). Haploinsufficiency of the transcription factors FOXC1 and FOXC2 results in aberrant ocular development. *Hum Mol Genet* **9**, 1021–1032.

Soriano, P. (1994). Abnormal kidney development and hematological disorders in PDGF beta-receptor mutant mice. *Gene Dev* **8**, 1888–1896.

Stuelsatz, P., Shearer, A., Li, Y., Muir, L. A., Ieronimakis, N., Shen, Q. W., Kirillova, I. and Yablonka-Reuveni, Z. (2015). Extraocular muscle satellite cells are high performance myo-engines retaining efficient regenerative capacity in dystrophin deficiency. *Dev Biol* **397**, 31–44.

Swinehart, I. T., Schlientz, A. J., Quintanilla, C. A., Mortlock, D. P. and Wellik, D. M. (2013). Hox11 genes are required for regional patterning and integration of muscle, tendon and bone. *Development* **140**, 4574–4582.

Taglietti, V., Kefi, K., Rivera, L., Bergiers, O., Cardone, N., Coulpier, F., Gioftsidi, S., Drayton-Libotte, B., Hou, C., Authier, F.-J., et al. (2023). Thyroid-stimulating hormone receptor signaling restores skeletal muscle stem cell regeneration in rats with muscular dystrophy. *Sci Transl Med* **15**, eadd5275.

Tajbakhsh, S., Rocancourt, D. and Buckingham, M. (1996). Muscle progenitor cells failing to respond to positional cues adopt non-myogenic fates in myf-5 null mice. *Nature* **384**, 266–270.

Tajbakhsh, S., Rocancourt, D., Cossu, G. and Buckingham, M. (1997). Redefining the Genetic Hierarchies Controlling Skeletal Myogenesis: Pax-3 and Myf-5 Act Upstream of MyoD. *Cell* **89**, 127–138.

Team, R. C. (2014). R: A language and environment for statistical computing. R Foundation for Statistical.

Terry, E. E., Zhang, X., Hoffmann, C., Hughes, L. D., Lewis, S. A., Li, J., Wallace, M. J., Riley, L., Douglas, C. M., Gutierrez-Montreal, M. A., et al. (2018). Transcriptional profiling reveals extraordinary diversity among skeletal muscle tissues. *eLife* **7**, e34613.

Tierney, M., Gromova, A., Sesillo, F., Sala, D., Spenlé, C., Orend, G. and Sacco, A. (2016). Autonomous Extracellular Matrix Remodeling Controls a Progressive Adaptation in Muscle Stem Cell Regenerative Capacity during Development. *Cell Reports* **14**, 1940–1952.

Tierney, M. T., Stec, M. J., Rulands, S., Simons, B. D. and Sacco, A. (2018). Muscle Stem Cells Exhibit Distinct Clonal Dynamics in Response to Tissue Repair and Homeostatic Aging. *Cell Stem Cell* **22**, 119-127.e3.

Tinevez, J.-Y., Perry, N., Schindelin, J., Hoopes, G. M., Reynolds, G. D., Laplantine, E., Bednarek, S. Y., Shorte, S. L. and Eliceiri, K. W. (2017). TrackMate: An open and extensible platform for single-particle tracking. *Methods* **115**, 80–90.

Uezumi, A., Fukada, S., Yamamoto, N., Takeda, S. and Tsuchida, K. (2010). Mesenchymal progenitors distinct from satellite cells contribute to ectopic fat cell formation in skeletal muscle. *Nat Cell Biol* **12**, 143–152.

Uezumi, A., Ikemoto-Uezumi, M. and Tsuchida, K. (2014). Roles of nonmyogenic mesenchymal progenitors in pathogenesis and regeneration of skeletal muscle. *Front. Physiol.* **5**, 68.

Urciuolo, A., Quarta, M., Morbidoni, V., Gattazzo, F., Molon, S., Grumati, P., Montemurro, F., Tedesco, F. S., Blaauw, B., Cossu, G., et al. (2013). Collagen VI regulates satellite cell self-renewal and muscle regeneration. *Nat. Commun.* **4**, 1964.

Vallejo, D., Hernández-Torres, F., Lozano-Velasco, E., Rodriguez-Outeiriño, L., Carvajal, A., Creus, C., Franco, D. and Aránega, A. E. (2018). PITX2 Enhances the Regenerative Potential of Dystrophic Skeletal Muscle Stem Cells. *Stem Cell Rep* **10**, 1398–1411.

Vartanian, A. D., Quétin, M., Michineau, S., Auradé, F., Hayashi, S., Dubois, C., Rocancourt, D., Drayton-Libotte, B., Szegedi, A., Buckingham, M., et al. (2019). PAX3 Confers Functional Heterogeneity in Skeletal Muscle Stem Cell Responses to Environmental Stress. *Cell Stem Cell* **24**, 958-973.e9.

Velthoven, C. T. J. van, Morree, A. de, Egner, I. M., Brett, J. O. and Rando, T. A. (2017). Transcriptional Profiling of Quiescent Muscle Stem Cells In Vivo. *Cell Reports* **21**, 1994–2004.

Verma, M., Fitzpatrick, K. R. and McLoon, L. K. (2017). Extraocular Muscle Repair and Regeneration. *Curr Ophthalmol Reports* **5**, 207–215.

Vicente-García, C., Hernández-Camacho, J. D. and Carvajal, J. J. (2022). Regulation of myogenic gene expression. *Exp. Cell Res.* **419**, 113299.

Wang, L., Siegenthaler, J. A., Dowell, R. D. and Yi, R. (2016). Foxc1 reinforces quiescence in self-renewing hair follicle stem cells. *Science* **351**, 613–617.

Whitesell, T. R., Chrystal, P. W., Ryu, J.-R., Munsie, N., Grosse, A., French, C. R., Workentine, M. L., Li, R., Zhu, L. J., Waskiewicz, A., et al. (2019). foxc1 is required for embryonic head vascular smooth muscle differentiation in zebrafish. *Dev Biol* **453**, 34–47.

Wickham, H. (2009). ggplot2, Elegant Graphics for Data Analysis.

Wolf, F. A., Angerer, P. and Theis, F. J. (2018). SCANPY: large-scale single-cell gene expression data analysis. *Genome Biol* **19**, 15.

Wright, W. E., Li, C., Zheng, C.-X. and Tucker, H. O. (2021). FOXP1 Interacts with MyoD to Repress its Transcription and Myoblast Conversion. *J. Cell. Signal.* **2**, 9–26.

Xi, H., Langerman, J., Sabri, S., Chien, P., Young, C. S., Younesi, S., Hicks, M., Gonzalez, K., Fujiwara, W., Marzi, J., et al. (2020). A Human Skeletal Muscle Atlas Identifies the Trajectories of Stem and Progenitor Cells across Development and from Human Pluripotent Stem Cells. *Cell Stem Cell* **27**, 158-176.e10.

Xie, N., Chu, S. N., Azzag, K., Schultz, C. B., Peifer, L. N., Kyba, M., Perlingeiro, R. C. R. and Chan, S. S. K. (2021). In vitro expanded skeletal myogenic progenitors from pluripotent stem cell-derived teratomas have high engraftment capacity. *Stem Cell Rep*.

Yang, Z., Jiang, S., Cheng, Y., Li, T., Hu, W., Ma, Z., Chen, F. and Yang, Y. (2017). FOXC1 in cancer development and therapy: deciphering its emerging and divergent roles. *Ther Adv Med Oncol* **9**, 797–816.

Yartseva, V., Goldstein, L. D., Rodman, J., Kates, L., Chen, M. Z., Chen, Y.-J. J., Foreman, O., Siebel, C. W., Modrusan, Z., Peterson, A. S., et al. (2020). Heterogeneity of Satellite Cells Implicates DELTA1/NOTCH2 Signaling in Self-Renewal. *Cell Reports* **30**, 1491-1503.e6.

Yennek, S., Burute, M., Théry, M. and Tajbakhsh, S. (2014). Cell Adhesion Geometry Regulates Non-Random DNA Segregation and Asymmetric Cell Fates in Mouse Skeletal Muscle Stem Cells. *Cell Reports* **7**, 961–970.

Yin, H., Price, F. and Rudnicki, M. A. (2013). Satellite cells and the muscle stem cell niche. *Physiol Rev* **93**, 23–67.

Yoshida, N., Yoshida, S., Koishi, K., Masuda, K. and Nabeshima, Y. (1998). Cell heterogeneity upon myogenic differentiation: down-regulation of MyoD and Myf-5 generates “reserve cells”. *J Cell Sci* **111 (Pt 6)**, 769–79.

Yoshioka, K., Nagahisa, H., Miura, F., Araki, H., Kamei, Y., Kitajima, Y., Seko, D., Nogami, J., Tsuchiya, Y., Okazaki, N., et al. (2021). Hoxa10 mediates positional memory to govern stem cell function in adult skeletal muscle. *Sci Adv* **7**, eabd7924.

Zacharias, A. L., Lewandoski, M., Rudnicki, M. A. and Gage, P. J. (2011). Pitx2 is an upstream activator of extraocular myogenesis and survival. *Dev Biol* **349**, 395–405.

Zakany, J. and Duboule, D. (2007). The role of Hox genes during vertebrate limb development. *Curr Opin Genet Dev* **17**, 359–366.

Zammit, P. S., Golding, J. P., Nagata, Y., Hudon, V., Partridge, T. A. and Beauchamp, J. R. (2004). Muscle satellite cells adopt divergent fates. *The Journal of Cell Biology* **166**, 347–357.

Zhang, P., Wong, C., Liu, D., Finegold, M., Harper, J. W. and Elledge, S. J. (1999). p21CIP1 and p57KIP2 control muscle differentiation at the myogenin step. *Gene Dev* **13**, 213–224.

FIGURE LEGENDS

Figure 1. Functional differences between EOM and TA MuSCs following activation.

A. Experimental scheme. Adult MuSCs isolated from *Tg:Pax7-nGFP* mice were plated in growth media (GM) and pulsed with EdU before fixation and immunostaining at Day (D) 3, D4, D5 and D10.

B. Immunofluorescence for MF20, PAX7 and EdU detection as per in A. Scale bar 100μm.

C-D. Bar plots of total number of nuclei and EdU+ nuclei represented as EOM/TA fold change (C) and percentage of EdU+ cells/total number of nuclei at D3, D4, D5. N>3 independent experiments with n≥3 mice per experiment.

E. Quantification of the percentage of Pax7+ cells/total number of nuclei at D10. n≥3 mice.

F. Quantification of the Fusion Index at D10. n=4 mice.

G. Experimental scheme. Live imaging of adult EOM and TA MuSCs from *Tg:Pax7-nGFP;Myog*^{ntdTom} from D3 *in vitro*.

H. Representative overlayed DIC and red fluorescence channel images at selected time points. Scale bar 25 μm.

I. Percentage of tdTom^{+} cells over total cell number at each timepoint. n=4 mice.

J. RT-qPCR on *in vitro* activated adult EOM and TA MuSCs for *Pax7*, *Myod*, *Myogenin* and *p21* normalized to *Rpl13*. n=8 mice.

K. Experimental scheme. Adult MuSCs from *Tg:Pax7-nGFP;Myog*^{ntdTom} mice were cultured for 5 days and re-sorted based on GFP and tdTom fluorescence for further analysis.

L. RT-qPCR for key myogenic markers of cells isolated as per in K. n=4 mice.

Data presented as mean ± SEM. Two-tailed unpaired Student's t-test; ns, non-significant, p-value>0.05, * p-value < 0.05, ** p-value<0.01, *** p-value < 0.005, **** p-value<0.0001. GM, growth media; DM, differentiation media.

Figure 2. Single cell transcriptome signatures of activated EOM and TA MuSCs.

A. sc-RNAseq pipeline for *in vitro* activated adult MuSCs.

B. UMAP visualization of EOM progenitors, EOM differentiating, TA progenitors, and TA differentiating clusters (left). Violin plots of the expression of myogenic markers *Pax7* (progenitor), *Myod* (committed) and *Myog* (differentiating) in each cluster (right).

C. Expression plots of myogenic markers.

D. Heatmap representing top differentially expressed genes in each cluster and expression levels across all cells.

E-F. Reactome pathway (E) and GO Molecular function (F) network analysis on top 100 DEGs of each cluster. Pie charts represent relative contribution of each cluster to this ontology term.

Figure 3. Molecular signature of EOM and TA quiescent MuSCs.

A. sc-RNAseq pipeline for quiescent adult MuSCs.

B. UMAP visualization of EOM and TA quiescent clusters.

C-D. Violin plot (C) and expression plot (D) of *Myf5*, *Pax7*, *Myod* and *Myog*.

E. Heatmap representing top differentially expressed genes in each cluster and expression levels across all cells.

F-G. Venn diagrams of the overlapping differentially expressed genes between quiescent and global *in vitro* activated datasets for EOM (F) and TA (G).

H-I. Expression plots of selected EOM (H) and TA (I) markers exclusive to Quiescence (Unique Q), common to quiescent and activated states (Conserved) and exclusive to activation (Unique Act) from the analysis in F-G.

Figure 4. EOM MuSC activation is accompanied by ECM remodelling.

A. Violin plots of matrisome scores for each cluster of the *in vitro* activated sc-RNAseq dataset.

B. Dot plot visualisation of differentially expressed matrisome components. ECM, extracellular matrix; A-P, affiliated proteins; PG, proteoglycans.

C. Immunofluorescence for Fibronectin (FN1), Collagen I (COLI), Collagen IV (COLIV) and PDGFRβ. Representative of N>2 different experiments. Scale bar 25 μm.

D. Western blot showing expression of CAV1, CAVIN1, MGP, MMP2, SPARC, IGFBP7 and H3 for normalization. Cells from n=3 mice pooled per lane.

E-F. Violin plot (E) and UMAP (F) of *Pdgfrb* expression on *in vitro* activated sc-RNAseq dataset.

G. Experimental scheme. MuSCs from adult *Tg:Pax7-nGFP* mice were activated *in vitro*, re-sorted based on their PDGFRβ expression and plated for further analysis.
H. Representative images of PDGFRβ positive and negative EOM MuSC fractions stained for MYOD, MYOGENIN and EdU as per in G. Scale bar 50 µm.
I-L. Quantification of number of cells/cm^2 (I) and percentage of EdU$^+$ (J), MYOD$^+$ (K) and MYOG$^+$ (L) cells. n=3 mice.
Data presented as mean ± SEM. Two-tailed unpaired Student's t-test; ns, non-significant, p-value>0.05, ** p-value<0.01, *** p-value < 0.005.

Figure 5. Distinct gene regulatory networks underlie EOM and TA activation dynamics.
A. Top 4 regulon activity for each cluster of the *in vitro* activated adult sc-RNAseq dataset overlaid onto UMAP representation.
B. Heatmap of Top 7 regulons in each cluster with activity level in each cell. Myod1_(+) appears twice as it is a regulon of both EOM Diff and TA Diff subpopulations.
C. Transcription factor network highlighting top regulons of each cluster as well as common regulons (35 regulons maximum). Proximity of the nodes in the network indicates a higher number of shared edges, highlighting core modules.

Figure 6. EOM properties are retained despite several passages *in vitro.*
A. Scheme of isolation and passages of EOM and TA adult MuSCs. Cells from *Tg:Pax7-nGFP;Myog^{ntdTom}* were cultured for 3 days (Act) and the entire wells passaged (P1, P2) every 3 days.
B. Normalized cell number ratios from experiment in A. Total cell numbers per well were counted at day 3 (D3), days 5 (D5) and upon passages (P) and normalized on the averaged EOM cell number in all wells at each time point. n=3 mice.
C. Ratio of tdTom$^+$/GFP$^+$ cells per time point obtained through FACS analysis of *Tg:Pax7-nGFP;Myog^{ntdTom}* EOM and TA adult MuSCs at D5, P1 and P2. n≥3 mice.
D. RT-qPCR at D3 (Act, Activated), P1 and P2 on whole cell populations for key myogenic markers, regulon TFs and matrisome genes identified in EOM progenitors isolated from adult *Tg:Pax7-nGFP* mice. n=4 mice.
E-F. Western blot for TFs (E) and matrisome genes (F) on total P2 population from EOM and TA MuSCs isolated from adult *Tg:Pax7-nGFP* mice. ACTIN and TUBULIN were used for normalization of protein loading. n=3 mice.
G. Densitometric analysis of the Western Blots in E-F.
Data presented as mean ± SEM. Two-tailed unpaired Student's t-test; ns, non-significant, p-value>0.05, * p-value < 0.05, ** p-value<0.01, *** p-value < 0.005.

Figure 7. EOM activated features are present during postnatal growth and can be modulated by FOXC1.
A. Scheme of isolation of EOM and TA MuSCs from *Tg:Pax7-nGFP;Myog^{ntdTom}* from postnatal day (P)7-P10 mice.
B. RT-qPCR on GFP$^+$/tdTom$^-$ cells. n>3 mice.
C-D. Immunostaining for FOXC1, tdTom (TOM) and DYSTROPHIN on cryosections from EOM and TA muscles isolated from P10 (C) and adult (D) *Pax7^{CreERT2}:R26^{tdTom}* mice. White arrowheads point to PAX7+FOXC1+ cells. Black arrowheads point to PAX7+FOXC1-cells. Scale bars 50µm.
E. Quantification of the experiment in D. n=4 mice.
F. Scheme of lentivirus transduction for FOXC1 gain of function (GOF) experiments on adult TA MuSCs. The transduced cells (mCherry+) were re-isolated by FACS or directly analysed in mixed cultures.
G-H. FACS plots of adult *Tg:Pax7-nGFP* TA MuSCs transduced with control (G) or GOF FOXC1 (H) virus at D5. Both viruses carry an mCherry reporter.
I. Western blot of transduced adult TA MuSCs for mCherry and Foxc1. VINCULIN was used for normalisation of protein loading. n≥3 mice.
J. RT-qPCR of transduced adult TA MuSCs for Myogenic Markers, Regulon Transcription factors (TFs) and key ECM proteins and regulators identified in EOM progenitors. n≥3 mice.
K-K'. Immunostaining of transduced adult TA MuSCs for FOXC1, EdU and Cell Mask Blue (CM-Blue, cytoplasmic stain). Scale bar 100µm.

L. Immunostaining of transduced adult TA MuSCs grown in differentiation media for 48h and stained for MF20. Scale bar 100μm.

M. Quantification of the Fusion Index for the images in L. n=4 mice.

N-U. Quantification of cellular properties of adult TA MuSCs in mixed cultures containing transduced and non-transduced cells. (N, R) Violin plots showing the single cell distribution of FOXC1 fluorescence intensity. Bar plots of quantification of nucleus area (O, S), total number of nuclei (P, T) and percentage of EdU+ nuclei (Q, U). For N-Q n≥4 mice, R-U n≥3 mice. Dashed bar in P indicates total output in the mixed culture irrespective of FOXC1 expression.

V-Y. Quantification of live imaging of adult TA MuSCs in mixed cultures containing transduced and non-transduced cells. Brightfield and red fluorescent channel images were acquired at 4 different timepoints (+12, +24, +36, +48 hours) post transduction. (V-Y) Quantification of the relative abundance of mCherry+ and mCherry- cells (V) at 12h time point (t) and cell density (V,W) at all timepoints from movie images. n=3 mice.

Z. Proposed model of the role of FOXC1 upon overexpression in TA MuSCs (TA GOF with re-sorting; TA GOF w/o re-sorting) and endogenously in EOM MuSCs.

Data presented as mean ± SEM. Two-tailed unpaired Student's t-test except in S,U where p values were obtained using one-way ANOVA with Tukey's post hoc; ns, non-significant, p-value>0.05, * p-value < 0.05, ** p-value<0.01,*** p-value < 0.005, **** p-value<0.0001. GM, growth media; DM, differentiation media.

Figure 8. RNA velocity reveals distinct population kinetics and potential key regulators of progenitor maintenance.

A. Number of regulatory links between regulons and matrisome genes depending on the number of top regulons in EOM and TA *in vitro* activated sc-RNAseq datasets.

B. Ratio of number of regulations of matrisome genes between EOM and TA adult *in vitro* activated MuSCs. Maximal difference for top 5 first regulons.

C. Heatmap of top regulons in global *in vitro* activated sc-RNAseq dataset with activity level in each cell.

D-E. Velocity streams overlaid onto a UMAP representation for EOM (D) and TA (E), along with expression patterns of *Myog* and *Pax7* on *in vitro* activated adult sc-RNAseq dataset.

F-G. Heatmap of driver gene expression from the velocity strems in D-E.

H. Experimental scheme. MuSCs isolated from adult *Tg:Pax7-nGFP* mice were cultured for 3 days to obtain EOM and TA conditioned media (CM). Hindlimb MuSCs were left untreated (control) or treated with CM from D1 to D4 post plating and pulsed with EdU 2h before fixation.

I-J. Quantification of number of nuclei normalised on initial cell number (I) and percentage of EdU+ nuclei (J) of hindlimb MuSCs treated as per in H. N≥2 independent experiments with n≥2 mice each. Different symbol per experiment.

K. Immunostaining of *Myf5^{nlacZ};Pdgfra^{H2BGFP}* P3 mouse head cryosections for β-galactosidase (β-gal) and GFP. Scale bar 500μm. Higher magnifications in K'-K''. Scale bar 100μm.

L. Quantification of the number of β-gal+ GFP+ cells per mm^2 in head muscles. n=3 mice.

Data presented as mean ± SEM. p values were obtained using one-way ANOVA with Tukey's post hoc; ns, non-significant, p-value>0.05, ** p-value<0.01, *** p-value < 0.005, **** p-value<0.0001.

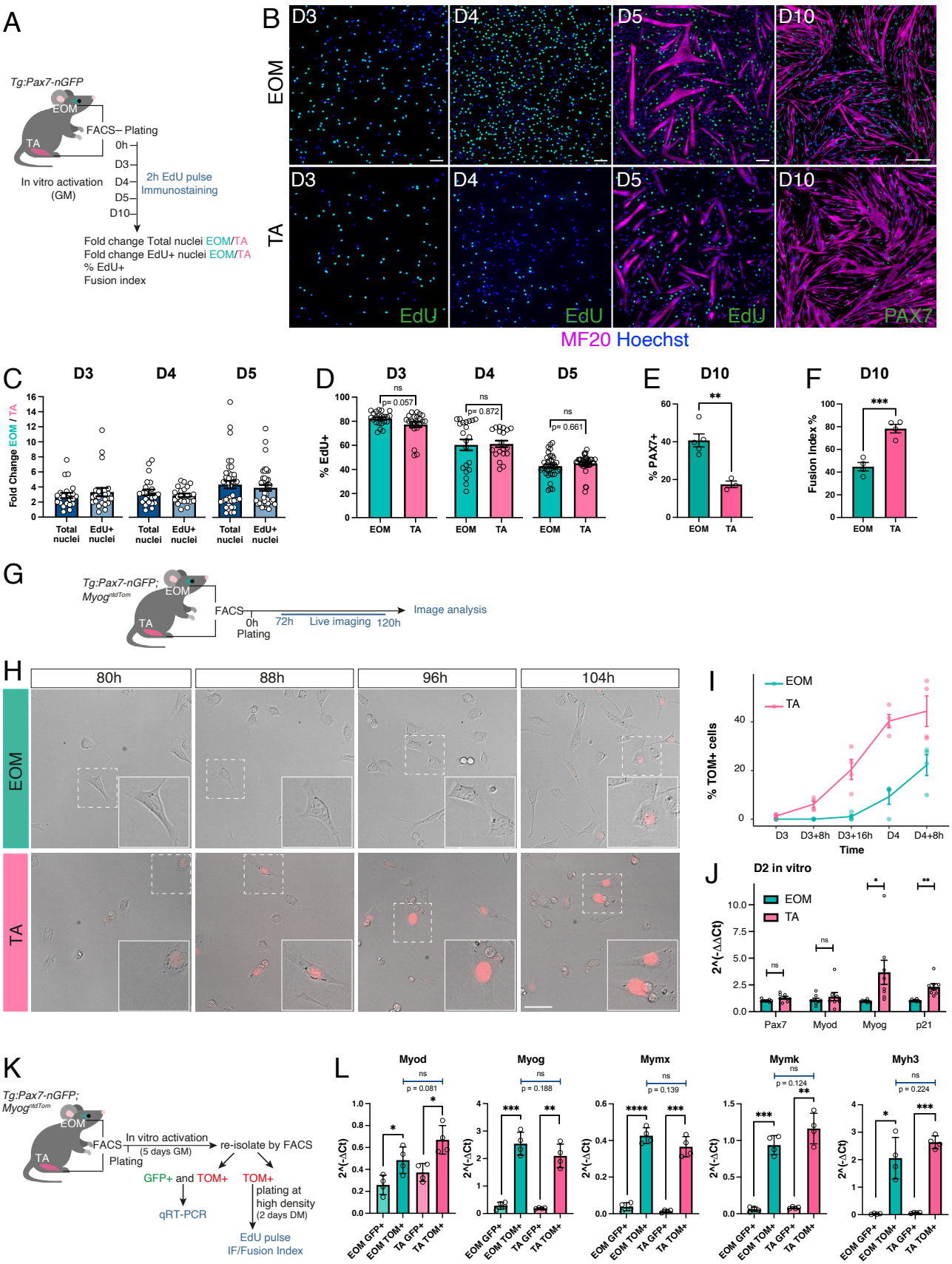
A
Tg:Pax7-nGFP
EOM
TA
FACS– Plating
0h
D3
D4
D5
D10
In vitro activation (GM)
2h EdU pulse Immunostaining
Fold change Total nuclei EOM/TA
Fold change EdU+ nuclei EOM/TA
% EdU+
Fusion index
B
D3
D4
D5
D10
EOM
TA
EdU
PAX7
MF20 Hoechst
C
D3
D4
D5
Fold Change EOM / TA
Total nuclei
EdU+ nuclei
D
D3
D4
D5
% EdU+
p= 0.057
p= 0.872
p= 0.661
ns
EOM
TA
E
D10
% PAX7+
**
F
D10
Fusion Index %
***
G
Tg:Pax7-nGFP; Myog ntdTom
FACS
0h Plating
72h
Live imaging
120h
Image analysis
H
80h
88h
96h
104h
EOM
TA
I
EOM
TA
% TOM+ cells
D3
D3+8h
D3+16h
D4
D4+8h
Time
J
D2 in vitro
2^(-ΔΔCt)
Pax7
Myod
Myog
p21
K
Tg:Pax7-nGFP; Myog ntdTom
FACS
Plating
In vitro activation (5 days GM)
re-isolate by FACS
GFP+ and TOM+
qRT-PCR
TOM+
plating at high density (2 days DM)
EdU pulse IF/Fusion Index
L
Myod
Myog
Mymx
Mymk
Myh3
2^(-ΔCt)
p = 0.081
p = 0.188
p = 0.139
p = 0.124
p = 0.224
EOM GFP+
EOM TOM+
TA GFP+
TA TOM+

Figure 2

Di Girolamo et al.

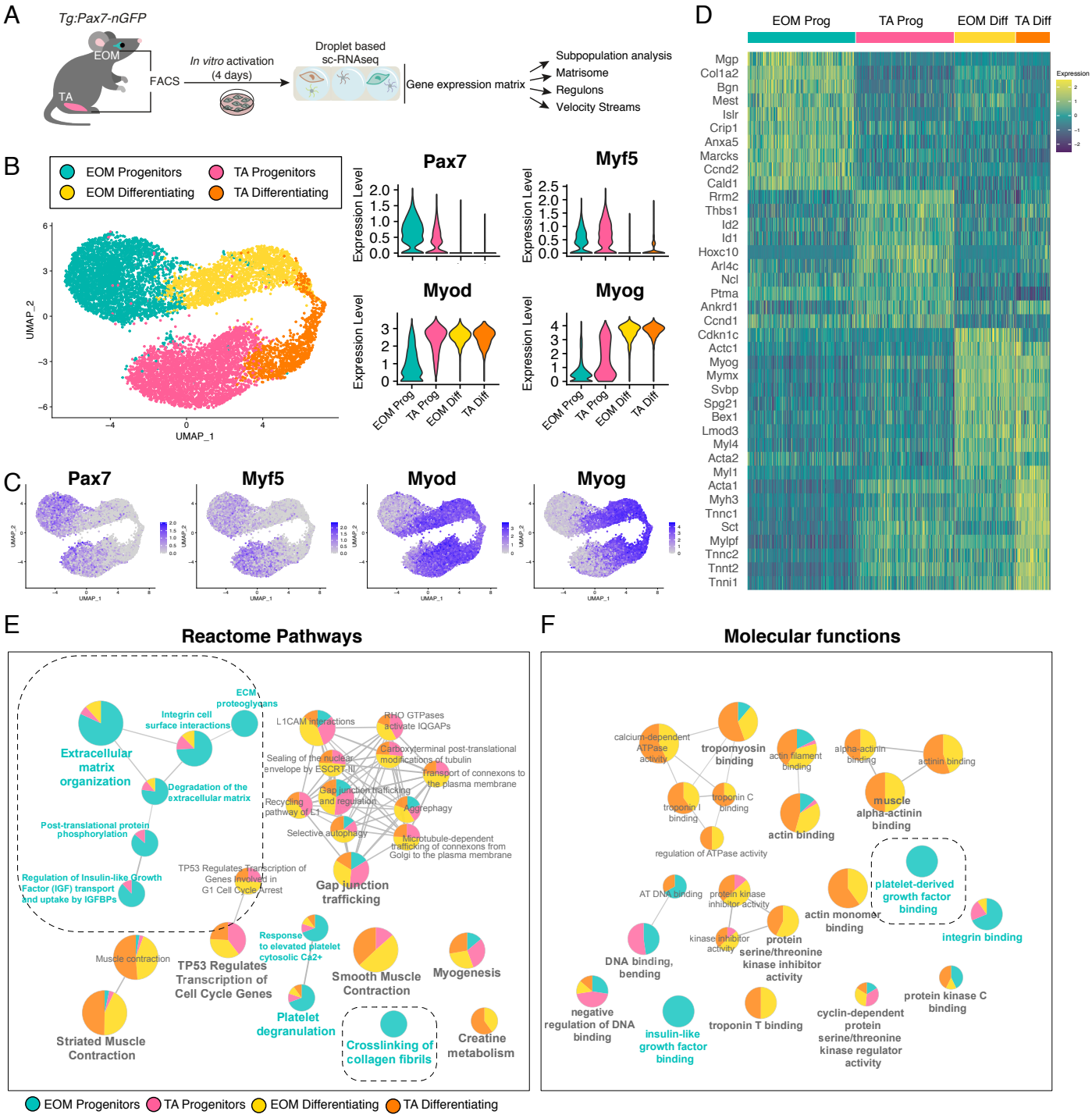

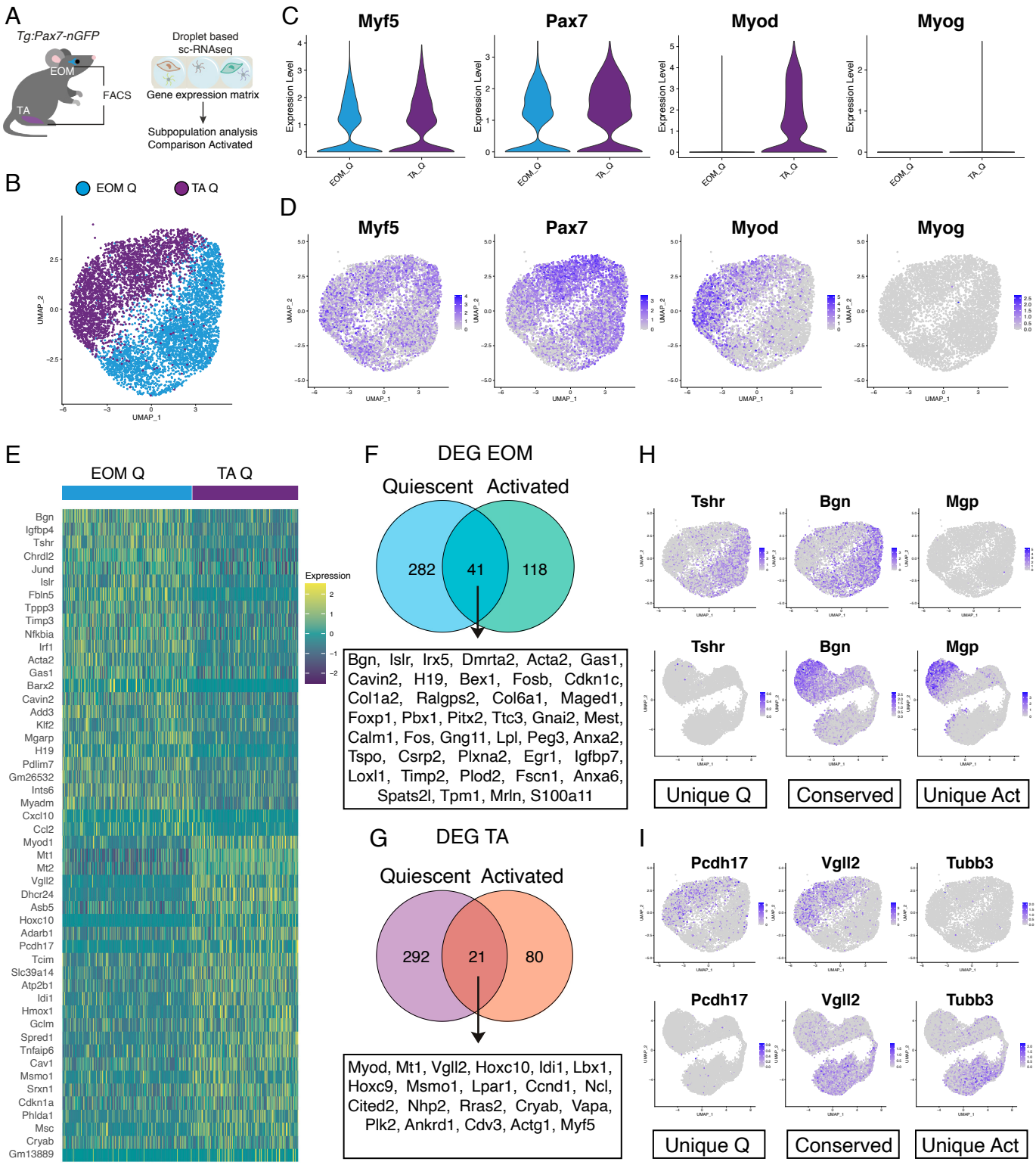
A
Tg:Pax7-nGFP
EOM
TA
FACS
Droplet based sc-RNAseq
Gene expression matrix
Subpopulation analysis Comparison Activated
B
EOM Q
TA Q
UMAP_1
UMAP_2
C
Myf5
Pax7
Myod
Myog
Expression Level
EOM_Q
TA_Q
D
Myf5
Pax7
Myod
Myog
UMAP_1
UMAP_2
E
EOM Q
TA Q
Bgn
Igfbp4
Tshr
Chrdl2
Jund
Islr
Fbln5
Tppp3
Timp3
Nfkbia
Irf1
Acta2
Gas1
Barx2
Cavin2
Add3
Klf2
Mgarp
H19
Pdlim7
Gm26532
Ints6
Myadm
Cxcl10
Ccl2
Myod1
Mt1
Mt2
Vgll2
Dhcr24
Asb5
Hoxc10
Adarb1
Pcdh17
Tcim
Slc39a14
Atp2b1
Idi1
Hmox1
Gclm
Spred1
Tnfaip6
Cav1
Msmo1
Srxn1
Cdkn1a
Phlda1
Msc
Cryab
Gm13889
Expression
F
DEG EOM
Quiescent Activated
282
41
118
Bgn, Islr, Irx5, Dmrta2, Acta2, Gas1, Cavin2, H19, Bex1, Fosb, Cdkn1c, Col1a2, Ralgps2, Col6a1, Maged1, Foxp1, Pbx1, Pitx2, Ttc3, Gnai2, Mest, Calm1, Fos, Gng11, Lpl, Peg3, Anxa2, Tspo, Csrp2, Plxna2, Egr1, Igfbp7, Loxl1, Timp2, Plod2, Fscn1, Anxa6, Spats2l, Tpm1, Mrln, S100a11
G
DEG TA
Quiescent Activated
292
21
80
Myod, Mt1, Vgll2, Hoxc10, Idi1, Lbx1, Hoxc9, Msmo1, Lpar1, Ccnd1, Ncl, Cited2, Nhp2, Rras2, Cryab, Vapa, Plk2, Ankrd1, Cdv3, Actg1, Myf5
H
Tshr
Bgn
Mgp
Unique Q
Conserved
Unique Act
I
Pcdh17
Vgll2
Tubb3
Unique Q
Conserved
Unique Act

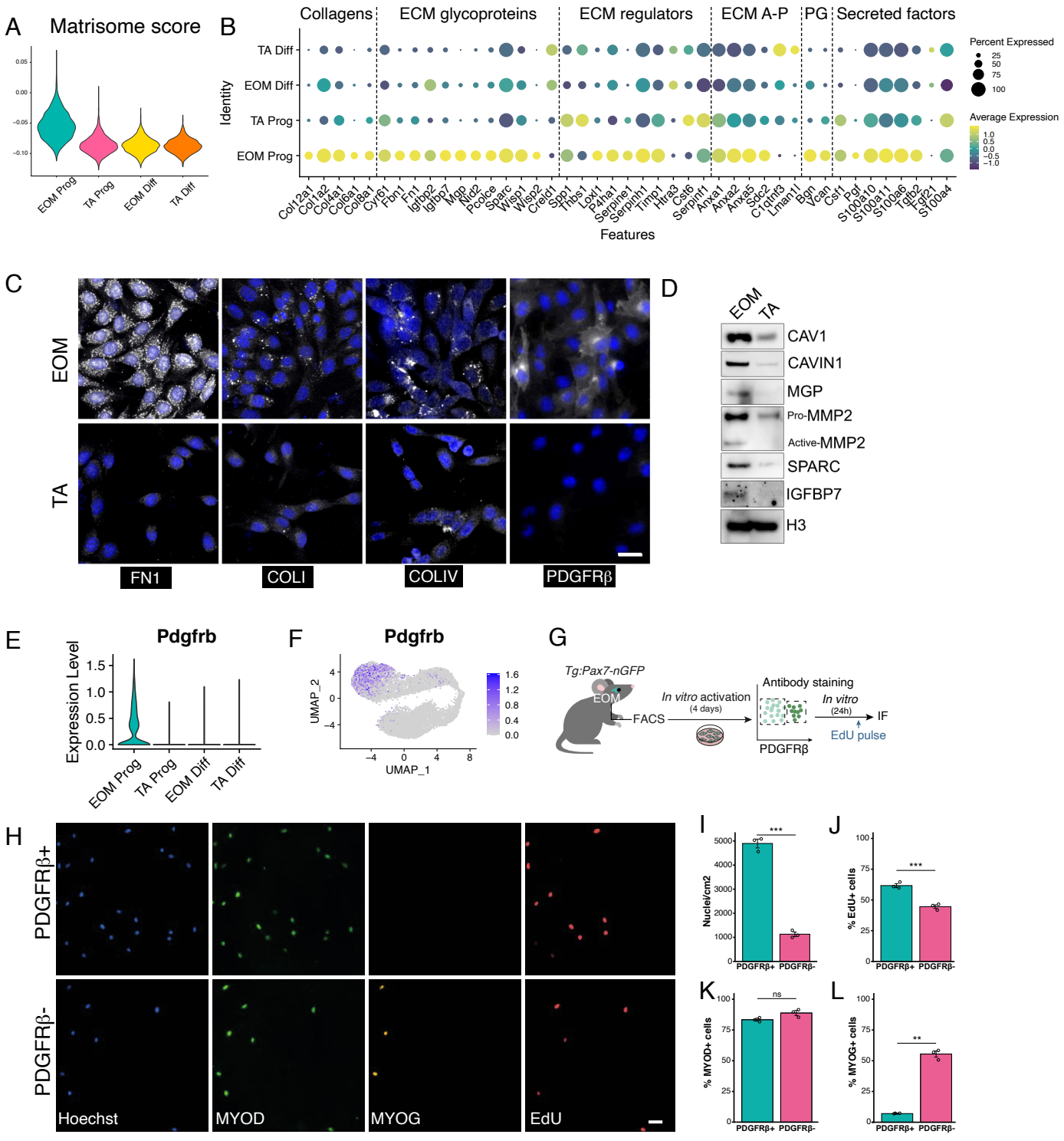
A
Matrisome score
EOM Prog
TA Prog
EOM Diff
TA Diff
B
Collagens
ECM glycoproteins
ECM regulators
ECM A-P
PG
Secreted factors
Identity
TA Diff
EOM Diff
TA Prog
EOM Prog
Features
Percent Expressed
Average Expression
C
EOM
TA
FN1
COLI
COLIV
PDGFRβ
D
EOM
TA
CAV1
CAVIN1
MGP
Pro-MMP2
Active-MMP2
SPARC
IGFBP7
H3
E
Pdgfrb
Expression Level
F
Pdgfrb
UMAP_2
UMAP_1
G
Tg:Pax7-nGFP
EOM
FACS
In vitro activation
(4 days)
Antibody staining
PDGFRβ
In vitro
(24h)
IF
EdU pulse
H
PDGFRβ+
PDGFRβ-
Hoechst
MYOD
MYOG
EdU
I
Nuclei/cm2
PDGFRβ+
PDGFRβ-
J
% EdU+ cells
K
% MYOD+ cells
ns
L
% MYOG+ cells

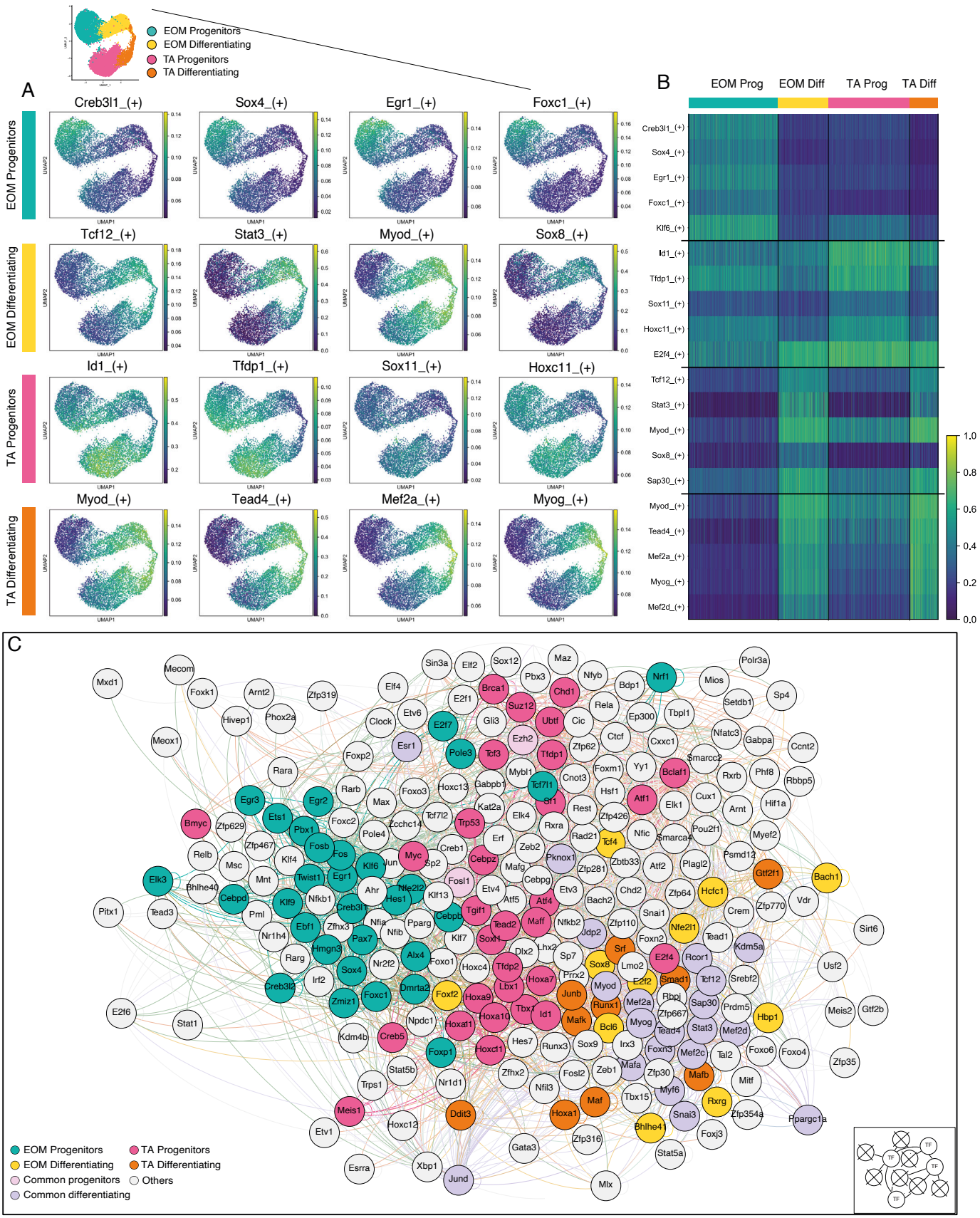
A
EOM Progenitors
EOM Differentiating
TA Progenitors
TA Differentiating
Creb3l1_(+)
Sox4_(+)
Egr1_(+)
Foxc1_(+)
Tcf12_(+)
Stat3_(+)
Myod_(+)
Sox8_(+)
Id1_(+)
Tfdp1_(+)
Sox11_(+)
Hoxc11_(+)
Myod_(+)
Tead4_(+)
Mef2a_(+)
Myog_(+)
UMAP1
UMAP2
B
EOM Prog
EOM Diff
TA Prog
TA Diff
Creb3l1_(+)
Sox4_(+)
Egr1_(+)
Foxc1_(+)
Klf6_(+)
Id1_(+)
Tfdp1_(+)
Sox11_(+)
Hoxc11_(+)
E2f4_(+)
Tcf12_(+)
Stat3_(+)
Myod_(+)
Sox8_(+)
Sap30_(+)
Myod_(+)
Tead4_(+)
Mef2a_(+)
Myog_(+)
Mef2d_(+)
1.0
0.8
0.6
0.4
0.2
0.0
C
EOM Progenitors
EOM Differentiating
Common progenitors
Common differentiating
TA Progenitors
TA Differentiating
Others
TF

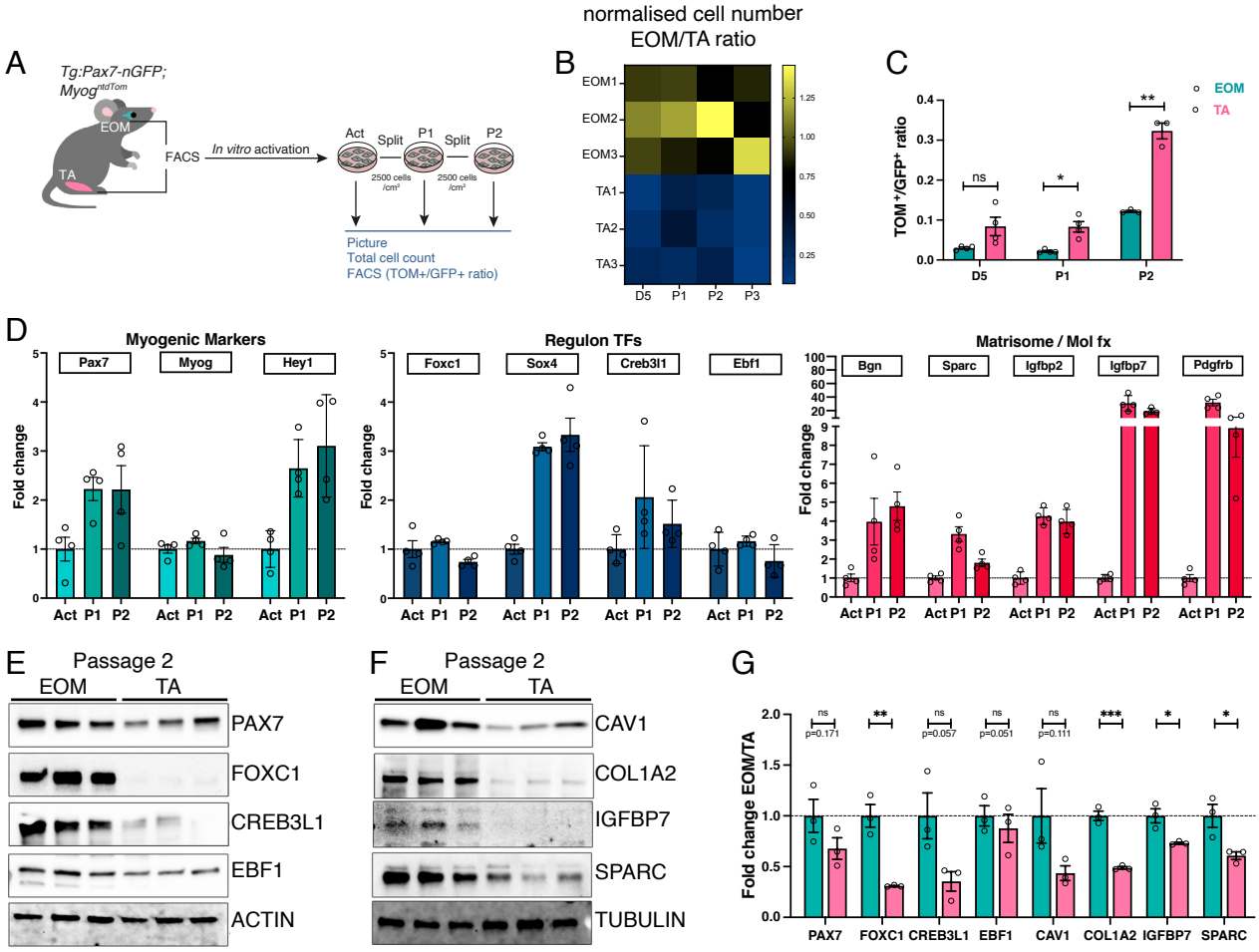
A
Tg:Pax7-nGFP;
Myog ntdTom
EOM
TA
FACS
In vitro activation
Act
Split
P1
Split
P2
2500 cells /cm²
2500 cells /cm²
Picture
Total cell count
FACS (TOM+/GFP+ ratio)
B
normalised cell number
EOM/TA ratio
EOM1
EOM2
EOM3
TA1
TA2
TA3
D5
P1
P2
P3
C
EOM
TA
TOM+/GFP+ ratio
ns
*
**
D5
P1
P2
D
Myogenic Markers
Pax7
Myog
Hey1
Regulon TFs
Foxc1
Sox4
Creb3l1
Ebf1
Matrisome / Mol fx
Bgn
Sparc
Igfbp2
Igfbp7
Pdgfrb
Fold change
Act P1 P2
E
Passage 2
EOM
TA
PAX7
FOXC1
CREB3L1
EBF1
ACTIN
F
Passage 2
EOM
TA
CAV1
COL1A2
IGFBP7
SPARC
TUBULIN
G
Fold change EOM/TA
ns p=0.171
**
ns p=0.057
ns p=0.051
ns p=0.111
***
*
*
PAX7
FOXC1
CREB3L1
EBF1
CAV1
COL1A2
IGFBP7
SPARC

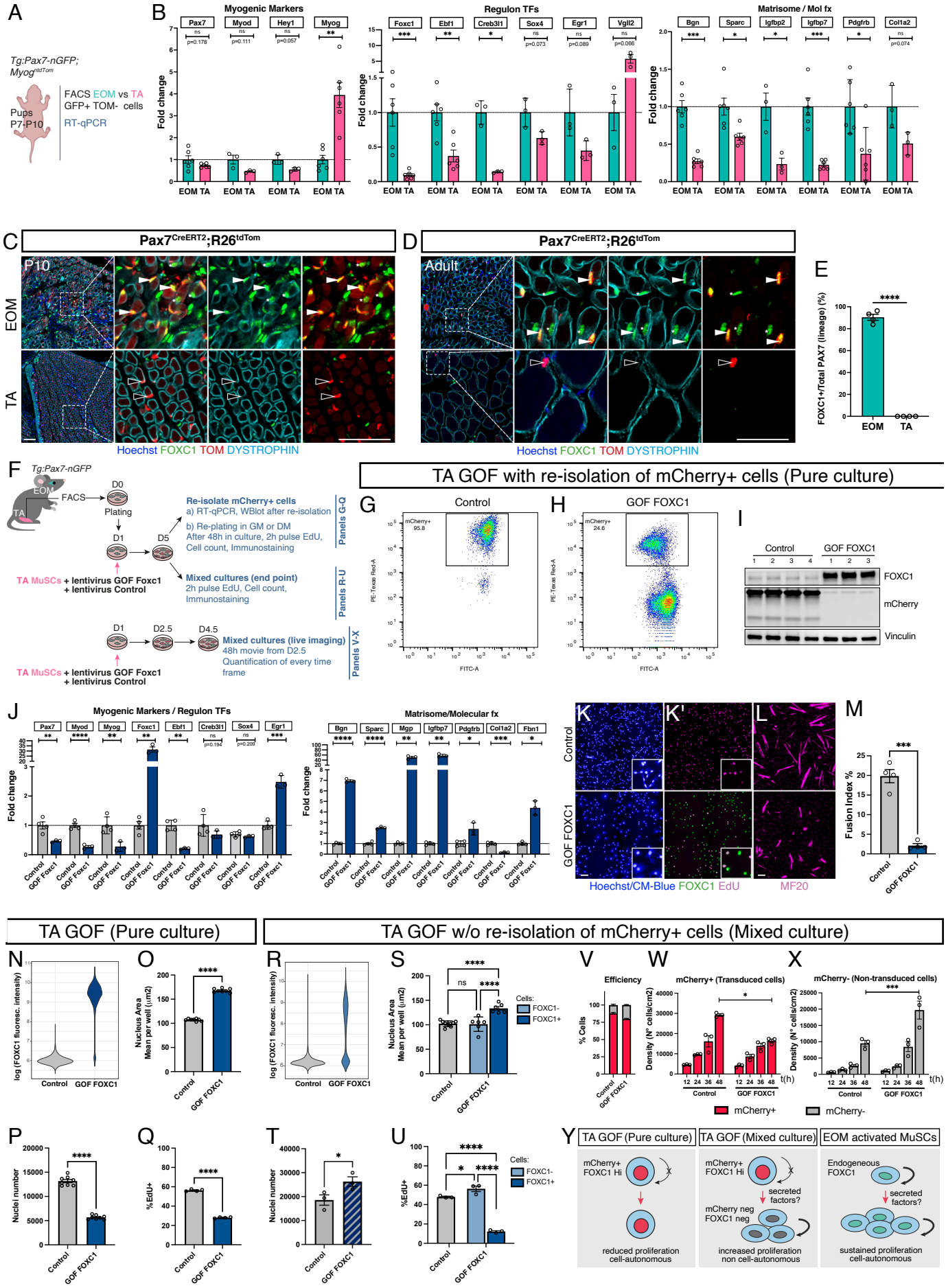
A
Tg:Pax7-nGFP;
Myog^tdTom
Pups
P7-P10
FACS EOM vs TA
GFP+ TOM- cells
RT-qPCR
B
Myogenic Markers
Pax7
Myod
Hey1
Myog
Regulon TFs
Foxc1
Ebf1
Creb3l1
Sox4
Egr1
Vgll2
Matrisome / Mol fx
Bgn
Sparc
Igfbp2
Igfbp7
Pdgfrb
Col1a2
Fold change
EOM TA
C
Pax7CreERT2;R26tdTom
P10
EOM
TA
Hoechst FOXC1 TOM DYSTROPHIN
D
Pax7CreERT2;R26tdTom
Adult
Hoechst FOXC1 TOM DYSTROPHIN
E
FOXC1+/Total PAX7 (lineage) (%)
EOM
TA
F
Tg:Pax7-nGFP
EOM
TA
FACS
D0
Plating
D1
D5
Re-isolate mCherry+ cells
a) RT-qPCR, WBlot after re-isolation
b) Re-plating in GM or DM
After 48h in culture, 2h pulse EdU,
Cell count, Immunostaining
Panels G-Q
TA MuSCs + lentivirus GOF Foxc1
+ lentivirus Control
Mixed cultures (end point)
2h pulse EdU, Cell count,
Immunostaining
Panels R-U
D1
D2.5
D4.5
Mixed cultures (live imaging)
48h movie from D2.5
Quantification of every time
frame
Panels V-X
TA MuSCs + lentivirus GOF Foxc1
+ lentivirus Control
TA GOF with re-isolation of mCherry+ cells (Pure culture)
G
Control
mCherry+
95.8
PE-Texas Red-A
FITC-A
H
GOF FOXC1
mCherry+
24.6
I
Control
GOF FOXC1
FOXC1
mCherry
Vinculin
J
Myogenic Markers / Regulon TFs
Matrisome/Molecular fx
Fold change
Control
GOF Foxc1
K
K'
L
Control
GOF FOXC1
Hoechst/CM-Blue FOXC1 EdU MF20
M
Fusion Index %
Control
GOF FOXC1
TA GOF (Pure culture)
TA GOF w/o re-isolation of mCherry+ cells (Mixed culture)
N
log (FOXC1 fluoresc. intensity)
Control
GOF FOXC1
O
Nucleus Area
Mean per well (µm2)
R
S
Cells:
FOXC1-
FOXC1+
V
Efficiency
% Cells
W
mCherry+ (Transduced cells)
Density (N° cells/cm2)
t(h)
X
mCherry- (Non-transduced cells)
mCherry+
mCherry-
P
Nuclei number
Q
%EdU+
T
U
Y
TA GOF (Pure culture)
TA GOF (Mixed culture)
EOM activated MuSCs
mCherry+
FOXC1 Hi
reduced proliferation
cell-autonomous
mCherry+
FOXC1 Hi
secreted
factors?
mCherry neg
FOXC1 neg
increased proliferation
non cell-autonomous
Endogeneous
FOXC1
secreted
factors?
sustained proliferation
cell-autonomous

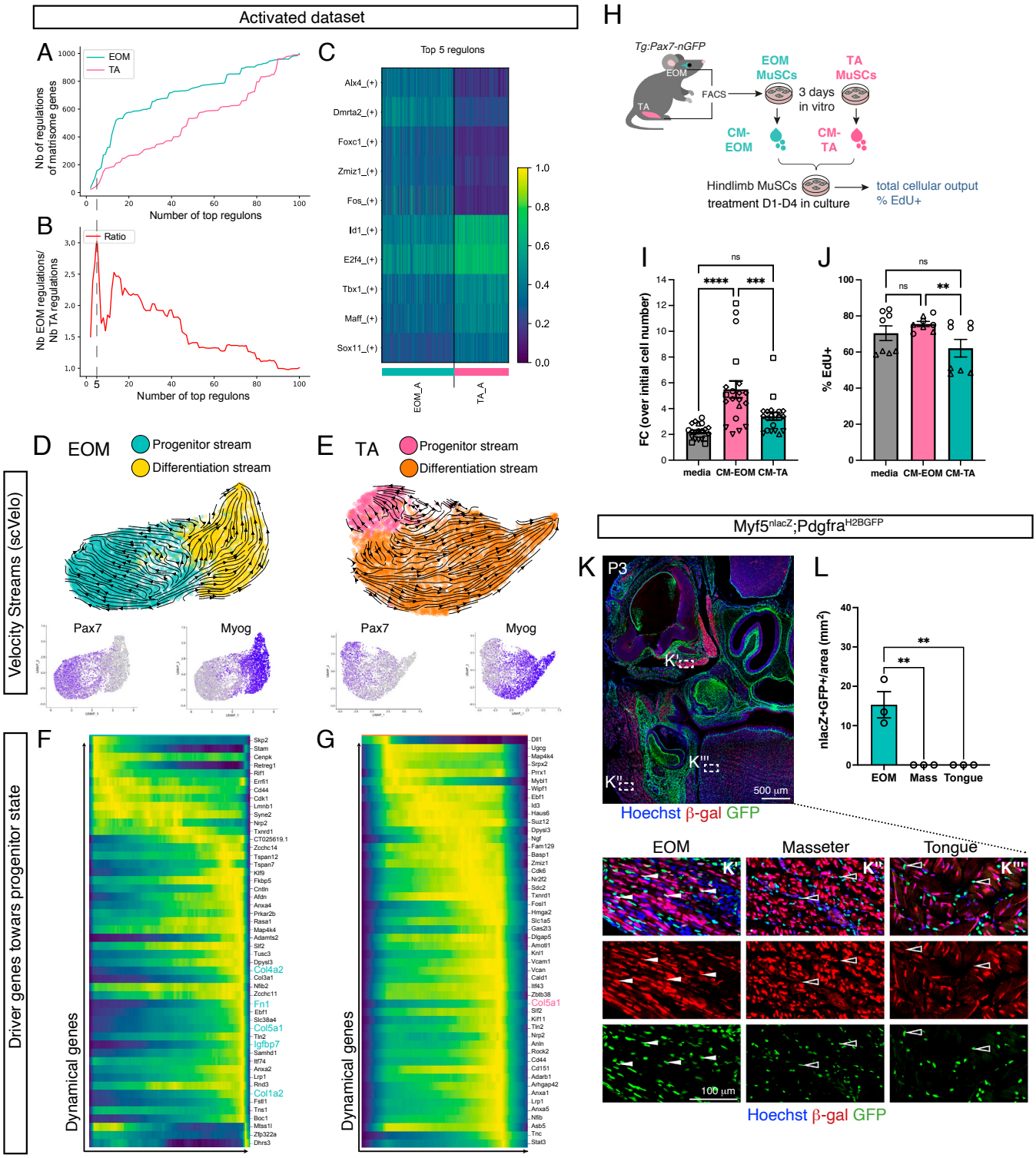
Activated dataset
A
EOM
TA
Nb of regulations of matrisome genes
Number of top regulons
B
Ratio
Nb EOM regulations/ Nb TA regulations
Number of top regulons
C
Top 5 regulons
Alx4_(+)
Dmrta2_(+)
Foxc1_(+)
Zmiz1_(+)
Fos_(+)
Id1_(+)
E2f4_(+)
Tbx1_(+)
Maff_(+)
Sox11_(+)
EOM_A
TA_A
H
Tg:Pax7-nGFP
EOM
TA
FACS
EOM MuSCs
TA MuSCs
3 days in vitro
CM-EOM
CM-TA
Hindlimb MuSCs treatment D1-D4 in culture
total cellular output % EdU+
I
FC (over initial cell number)
media
CM-EOM
CM-TA
J
% EdU+
media
CM-EOM
CM-TA
D
EOM
Progenitor stream
Differentiation stream
E
TA
Progenitor stream
Differentiation stream
Velocity Streams (scVelo)
Pax7
Myog
Pax7
Myog
Myf5nlacZ;PdgfraH2BGFP
K
P3
K'
K''
K'''
500 µm
Hoechst β-gal GFP
L
nlacZ+GFP+/area (mm2)
EOM
Mass
Tongue
EOM
Masseter
Tongue
100 µm
Hoechst β-gal GFP
F
Driver genes towars progenitor state
Dynamical genes
G
Dynamical genes